AD-A090 805 MARYLAND UNIV COLLEGE PARK DEPT OF PHYSICS AND ASTRONOMY F/G 20/1
INVESTIGATION OF NOISE IN SOLIDS AT LOW TEMPERATURES.(U)
AUG 80 W S DAVIS, K KRACK, J RICHARD, J WEBER F49620-77-C-0065
UNCLASSIFIED AFOSR-TR-80-1008 NL

1 OF 2
AD A 090805

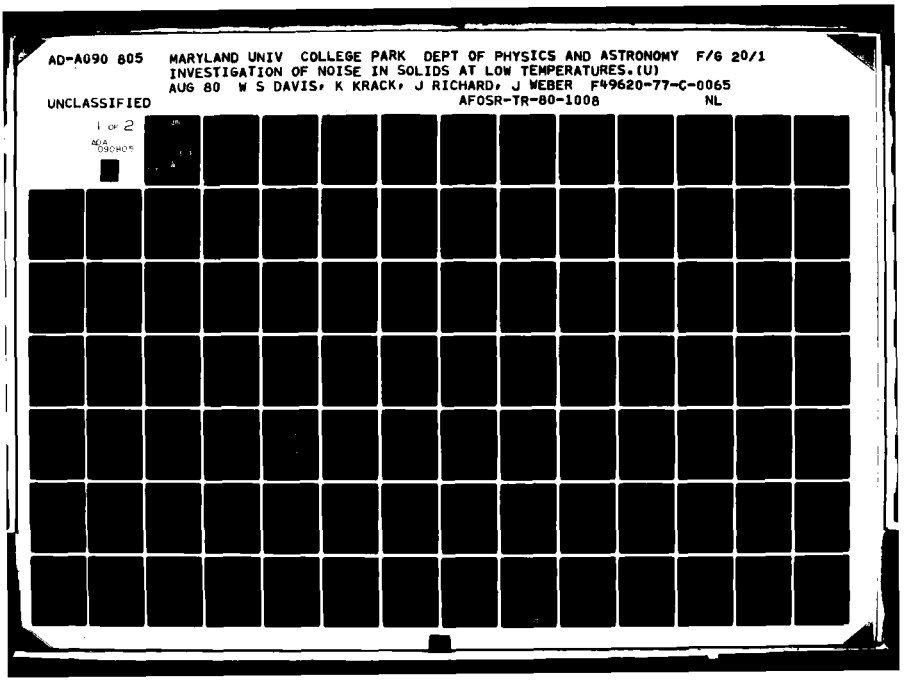

AFOSR-TR- 80 - 1008

LEVEL III

(3)

A070016

ANNUAL REPORT

To

AIR FORCE OFFICE OF SCIENTIFIC RESEARCH

On

INVESTIGATION OF NOISE IN SOLIDS AT LOW TEMPERATURES

Contract F49620-77-C-0065

August 1980

UNIVERSITY OF MARYLAND
DEPARTMENT OF PHYSICS AND ASTRONOMY
COLLEGE PARK, MARYLAND

UNCLASSIFIED

SECURITY CLASSIFICATION OF THIS PAGE (When Data Entered)

REPORT DOCUMENTATION PAGE	READ INSTRUCTIONS BEFORE COMPLETING FORM
1. REPORT NUMBER: AFOSR-TR-80-1008	2. GOVT ACCESSION NO.: AD-A090 805
4. TITLE (and Subtitle): Investigation of Noise in Solids at Low Temperatures.	5. TYPE OF REPORT & PERIOD COVERED: Annual Scientific Report 3/1/79 - 2/28/80
	6. PERFORMING ORG. REPORT NUMBER
7. AUTHOR(s): Wm. S. Davis / K. Krack / J.-P. Richard and J. Weber	8. CONTRACT OR GRANT NUMBER(s): F49620-77-C-0065
9. PERFORMING ORGANIZATION NAME AND ADDRESS: Department of Physics and Astronomy / University of Maryland / College Park, Maryland 20742	10. PROGRAM ELEMENT, PROJECT, TASK AREA & WORK UNIT NUMBERS: 61102F 2309 A1
11. CONTROLLING OFFICE NAME AND ADDRESS: Air Force Office of Scientific Research/NP / Bolling Air Force Base / Washington, D. C. 20332	12. REPORT DATE: August 1980
	13. NUMBER OF PAGES: 110
14. MONITORING AGENCY NAME & ADDRESS (if different from Controlling Office): 12 121	15. SECURITY CLASS. (of this report): Unclassified
	15a. DECLASSIFICATION DOWNGRADING SCHEDULE

16. DISTRIBUTION STATEMENT (of this Report):

Approved for public release; distribution unlimited.

9 Annual Rept. 1 Mar. 79 - 28 Feb. 80

17. DISTRIBUTION STATEMENT (of the abstract entered in Block 20, if different from Report):

18. SUPPLEMENTARY NOTES

19. KEY WORDS (Continue on reverse side if necessary and identify by block number)

20. ABSTRACT (Continue on reverse side if necessary and identify by block number)

This research is concerned with the theory and observations of fluctuation phenomena.

Observations have been made of the thermal fluctuations associated with the normal modes of oscillation of an aluminum cylinder at 4 Kelvin. A summary has been accepted by the Physical Review, and a preprint is included here.

219638

UNCLASSIFIED

UNCLASSIFIED

Progress has been made in solving the difficult problems associated with noise measurements in high quality factor ($Q \sim 10^8$ to 10^9) silicon and sapphire crystals. The present status is summarized, together with a description of a new large Dewar capable of cooling a large volume (35 liters) to 20 millikelvin).

A new approach has been discovered for increasing the interaction of weak forces with a detection system. This makes use of correlated quantum states.

In certain cases transition probabilities are proportional to the first power instead of the usual square of the interaction. This offers possibilities for enormous increases in transition rates. Preprints of two papers submitted for publication are included.

TABLE OF CONTENTS

Report Documentation Page i

Introduction 1

Measurement of Noise and Other Properties at Low Temperatures 2

Observation of Well Behaved Noise and Fluctuations in an Aluminum Cylinder at Liquid Helium Temperatures 29

New Approach to Detection of Small Signals 61

Exchange of Energy with Large Numbers of Particles 62

New Method for Increase of Interaction of Gravitational Radiation with an Antenna 69

Experiment to Search for Correlated State Effects 77

Design of the Milli-Kelvin Cryostat 78

Magnetic Levitation 83

Completion of the Gas Handling System 85

Appendix

INTRODUCTION

The sensitivity of measurements and the detection and observation of a number of phenomena are limited by the thermal noise which is generated within the passive and active electronics components. This kind of noise is expected to decrease as temperatures are lowered.

In this report we are concerned with low frequencies. Let $\hbar$ be Planck's constant divided by 2π, let k be Boltzmann's constant, let ω be the angular frequency and let T be the absolute temperature. ω is low for our purposes if

$$\omega << \frac{kT}{\hbar} = 1.6 \times 10^{11} T$$

At such low frequencies the thermal noise power is proportional to the temperature. Therefore, if we go from room temperature to .020 K, a decrease in thermal noise by a factor $\frac{.02}{300} = \frac{1}{15,000}$ is expected. This kind of improvement is realizable only if the associated instrumentation is correspondingly improved, and if new sources of noise do not appear. For these reasons considerable research and development is necessary. The associated instrumentation must be itself low noise and low temperature electronics. A major source of noise is usually the cryogenics installation since it involves boiling liquids, and large temperature gradients. Other possible noise sources include "frozen in" metastable configurations of a solid which slowly relax to the state of lowest free energy, giving rise to excess noise over an extended period.

For these reasons the exploration of noise at low temperatures requires a major research effort -- in cryogenics, in electronics, in the techniques of isolation and filtering, and continuation of the theory of the interaction of small forces with detection systems.

Measurement of Noise and Other Properties at Low Temperatures*

Wm. S. Davis

April 30, 1980

Introduction

The experimental work during the past year has consisted of some cooldowns with attempts to measure the noise and other properties of materials including silicon and sapphire at liquid helium temperatures.* Briefly, one experiment consists of two monocrystals, a 15 kg silicon crystal and a 5.2 kg sapphire crystal. Each is instrumented with a piezoelectric ceramic transducer, and each rests on an aluminum four point rigid suspension. Properties of the fundamental mode are observed with the transducers. These include the noise, frequency, and mechanical dissipation (the Q). Both crystals are in a single cryostat cooled to 4 to 5 Kelvin by a helium liquefier.

With the present signal coupling and preamplifier the silicon noise measurement was discovered to be impossible, practically speaking. Excess noise was measured in the sapphire (1000 Kelvin and above). This noise is now believed to be due to a mechanical instability of the crystal suspension which can be corrected. The Q and frequency measurements of silicon show interesting variations below 15 Kelvin. The data indicate that the Q might depend on the time derivative of the temperature as well as the temperature itself. Also, there is an unexpected variation in the frequency of the fundamental mode. These measurements will be repeated with active temperature control of the silicon.

*Background for this section may be found in last year's annual report. The relevant section is in the appendix of this report.

Properties of Silicon

The silicon is supported by a 6061 aluminum four point rigid suspension and instrumented with a piezoelectric ceramic transducer (pzt - 4) as shown in figure 1. The electronics used in the frequency and Q measurements are shown in figure 2. The silicon crystal is excited by driving it at the resonant frequency with the transducer. Once excited the crystal "rings" for a long time. During this ringing the transducer output is connected to a preamplifier which is a tuned cascode FET amplifier with CP 640 for the transistors. The lock-in amplifier is set in the vector mode, which produces the magniture of the input signal and the phase of the input signal with respect to the reference. A phase lock loop continuously adjusts the reference frequency generator, a quartz crystal voltage controlled oscillator, to maintain a zero phase difference. The phase lock loop has a damped second order response with respect to variations in phase. The circuit was originally assembled to demonstrate a silicon stabilized clock. So far the quartz crystal oscillator is more stable than the silicon itself, over a time interval of several hours or more. However, the same circuit is also useful in measuring the Q and frequency of the silicon. The magnitude of the silicon oscillation is recorded on a chart recorder. Decay times and Q's are then computed from the recordings. The period of the oscillation is read from an electronic counter which uses an oven stabilized crystal oscillator as its time base. The stability of this oscillator is rated at better than 5×10^{-10} per day.

Two resistance thermometers are epoxied into the aluminum base near the four point suspension. One is germanium and the other is platinum. Neither is calibrated very well with an error of as much as 25%. In the range where the sensitivities of the two devices overlap, 10 to 20 Kelvin,

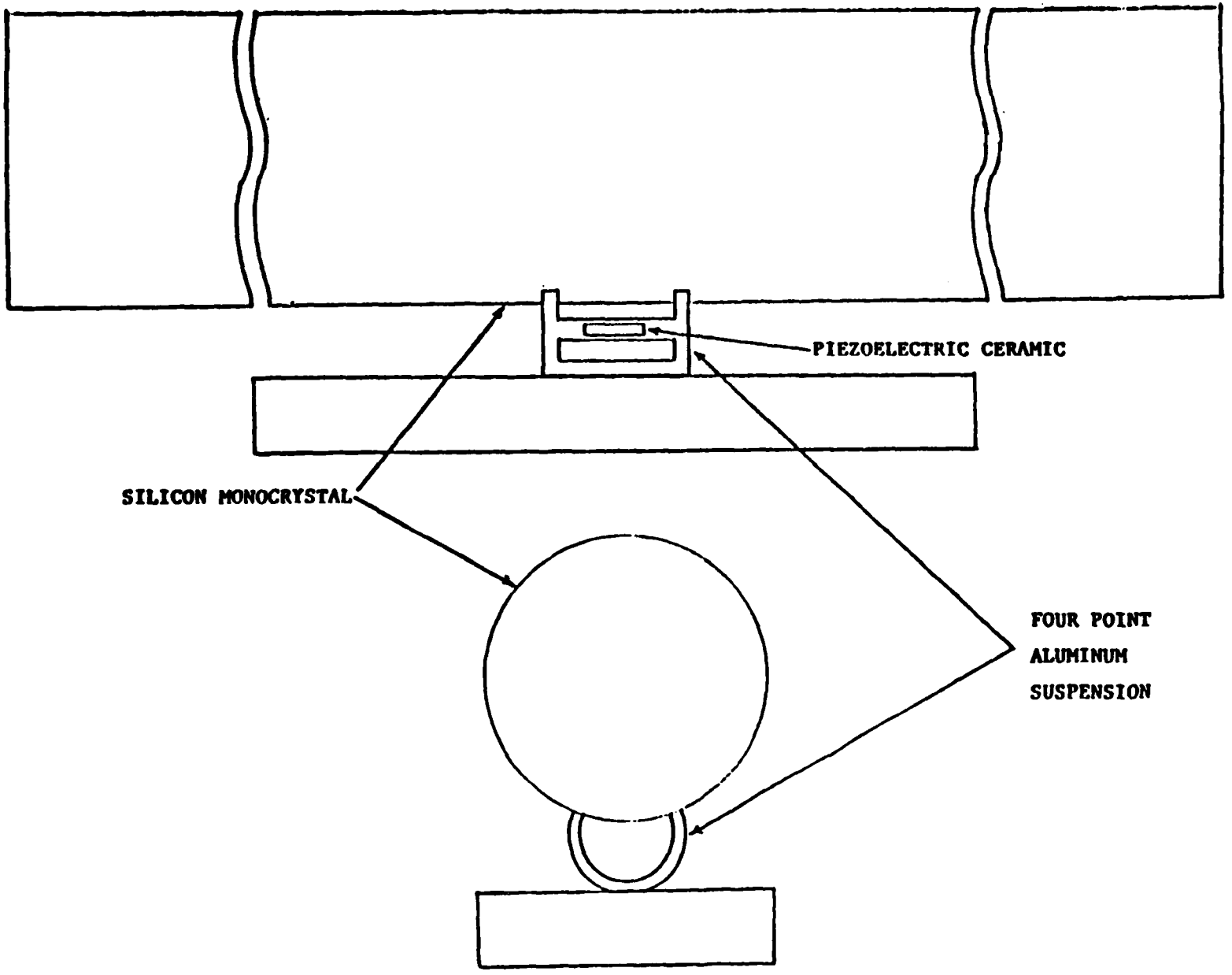

Figure 1. Aluminum four point suspension for 15 kg silicon crystal.

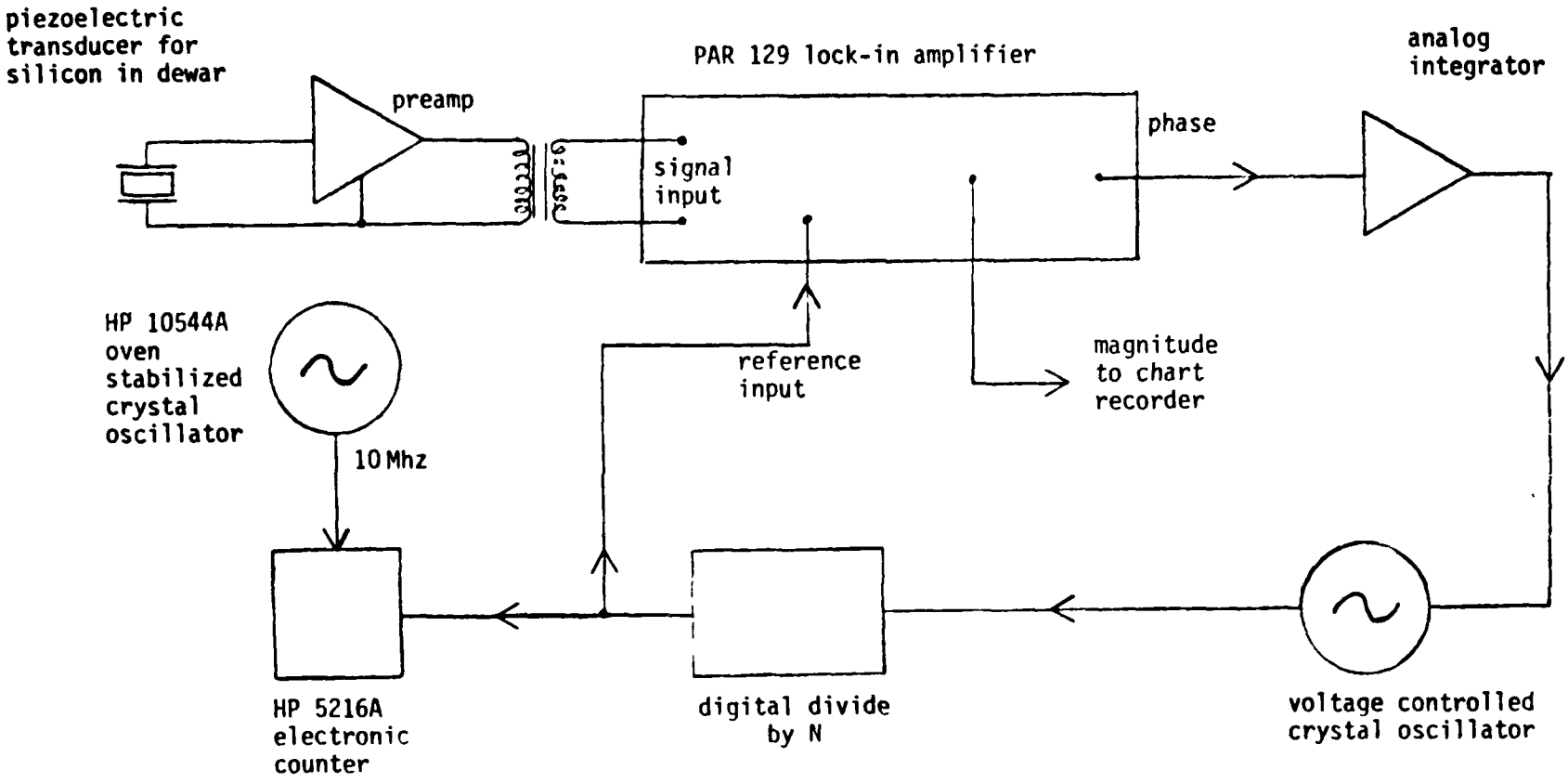

Figure 2. Electronics for silicon frequency and Q measurements.

they differ by 2 to 3 Kelvin. Because of this discrepancy, data taken with each device are kept separate.

Figure 3 shows measurements of Q of silicon from 4.3 to 18 Kelvin. This curve is similar to previous data as given in figure 4. In particular, there is a minimum at between 11 and 12 Kelvin. However, all these measurements were made as the crystal was warming up. The temperature was changing during each measurement. Figure 5 gives the temperature of the silicon as a function of date and time for the data of figure 3. Liquid helium was present in the dewar from before 9-29 until 11-4. On the latter date when the last of the liquid disappeared, the temperature of the silicon started to rise rapidly. The shape of the temperature verses time curve is essentially determined by the specific heats and thermal conductivities of the various components of the cryostat and is NOT strongly affected by the properties of the silicon crystal. Previous experiments have produced curves of similar shape. The time rate of change of the temperature at each temperature is given in figure 6. Note that the temperature at which the Q is a minimum is about the same as the temperature at which the rate of change of temperature is a maximum. The shape of the two curves, ie. figures 3 and 6, is suspiciously similar. It is possible that this is just a coincidence. Alternatively, the Q of the silicon crystal might depend at least partly on the rate of change of temperature. The obvious next step is to make the measurements of Q at constant temperature, and compare these with the previous measurements. An experiment with active temperature control at liquid helium temperatures has been assembled and will be ready for cooling in the near future. A drawing of the apparatus may be found in figure 7. The four point suspension is attached to an aluminum frame in which is imbedded heater resistors and temperature sensors. The

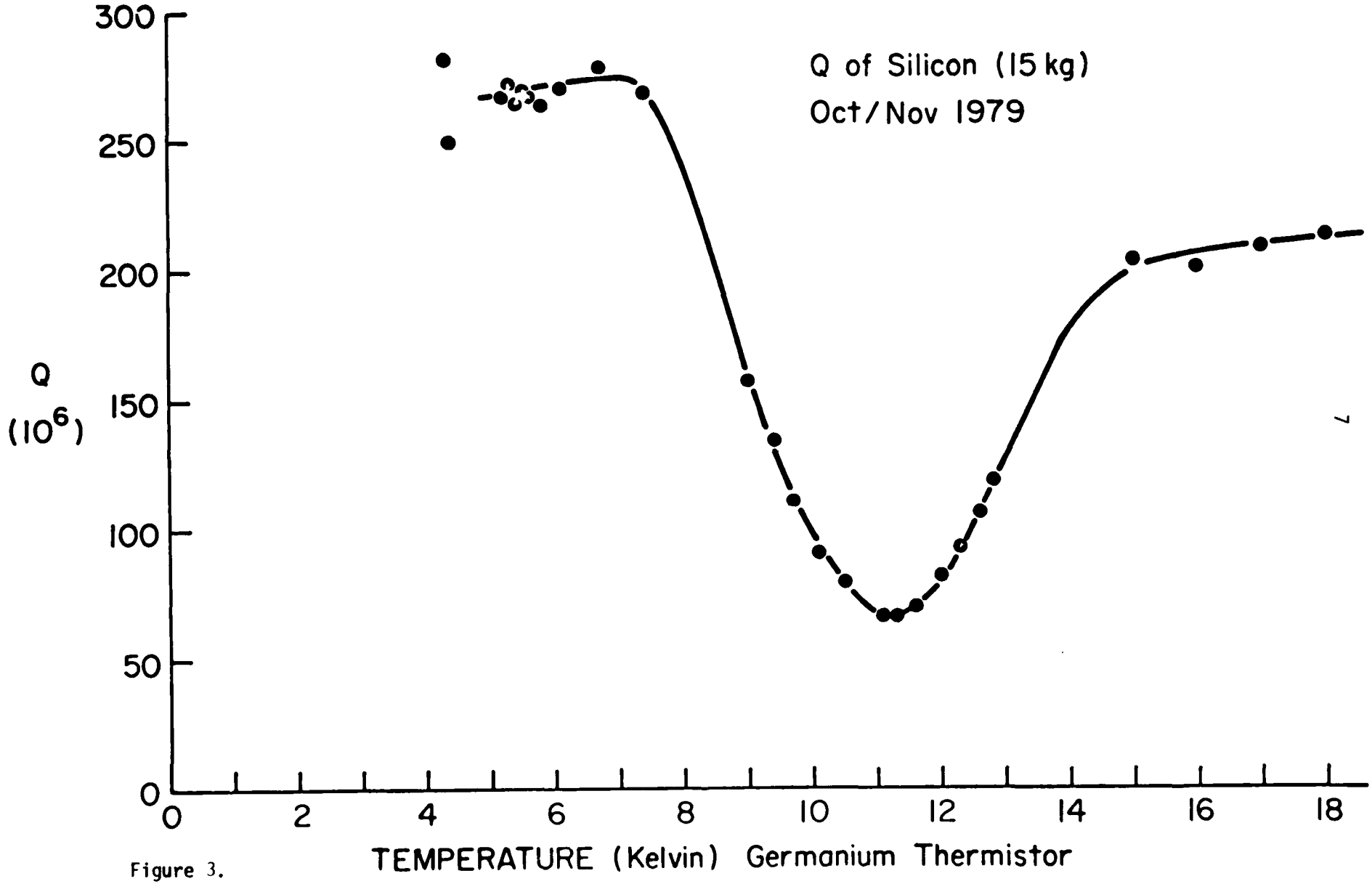
Q of Silicon (15 kg)
Oct/Nov 1979
Q
(10^6)
300
250
200
150
100
50
0
0
2
4
6
8
10
12
14
16
18
TEMPERATURE (Kelvin) Germanium Thermistor

Figure 3.

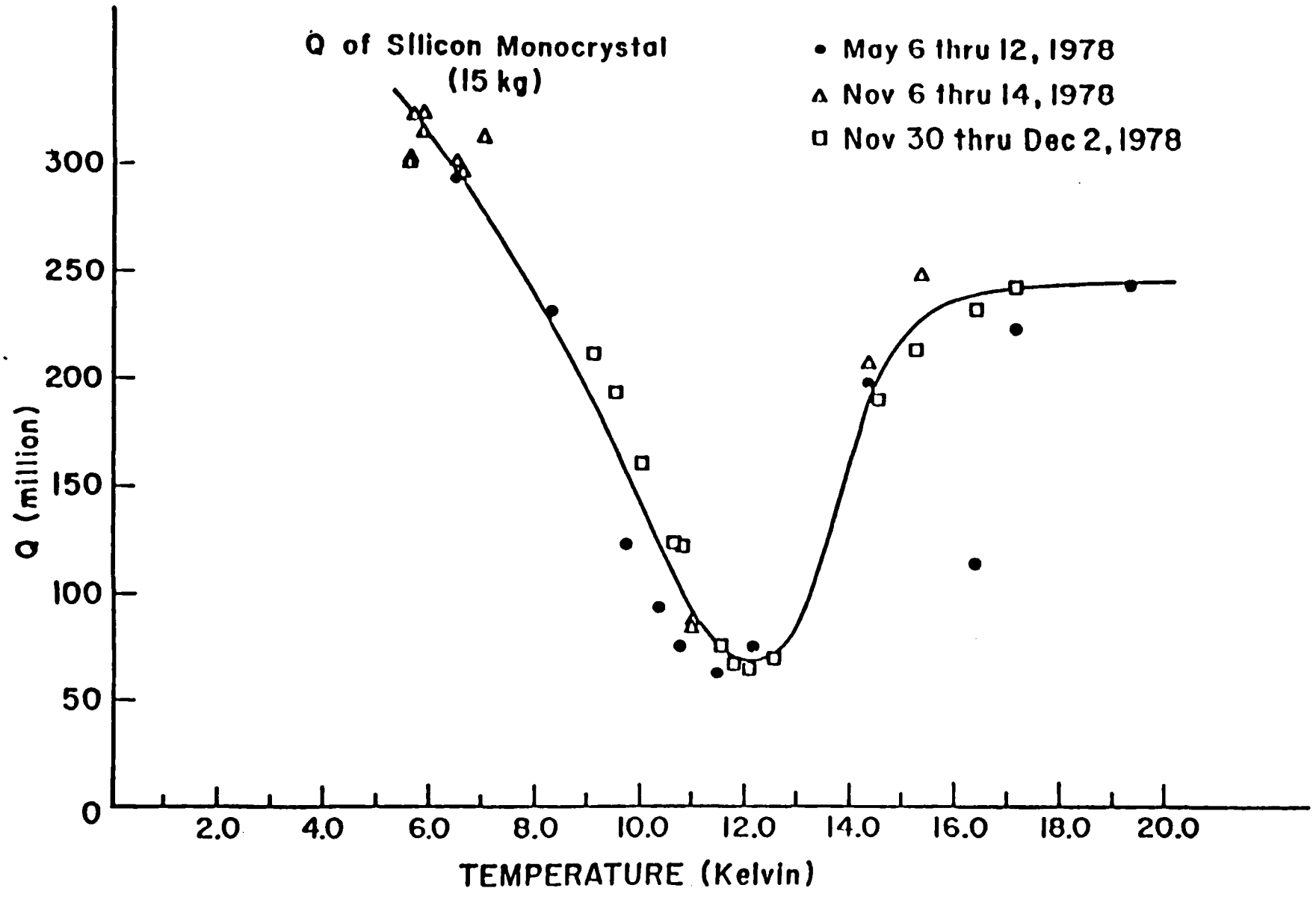

Figure 4. Q of longitudinal mode of 15 kg silicon crystal.

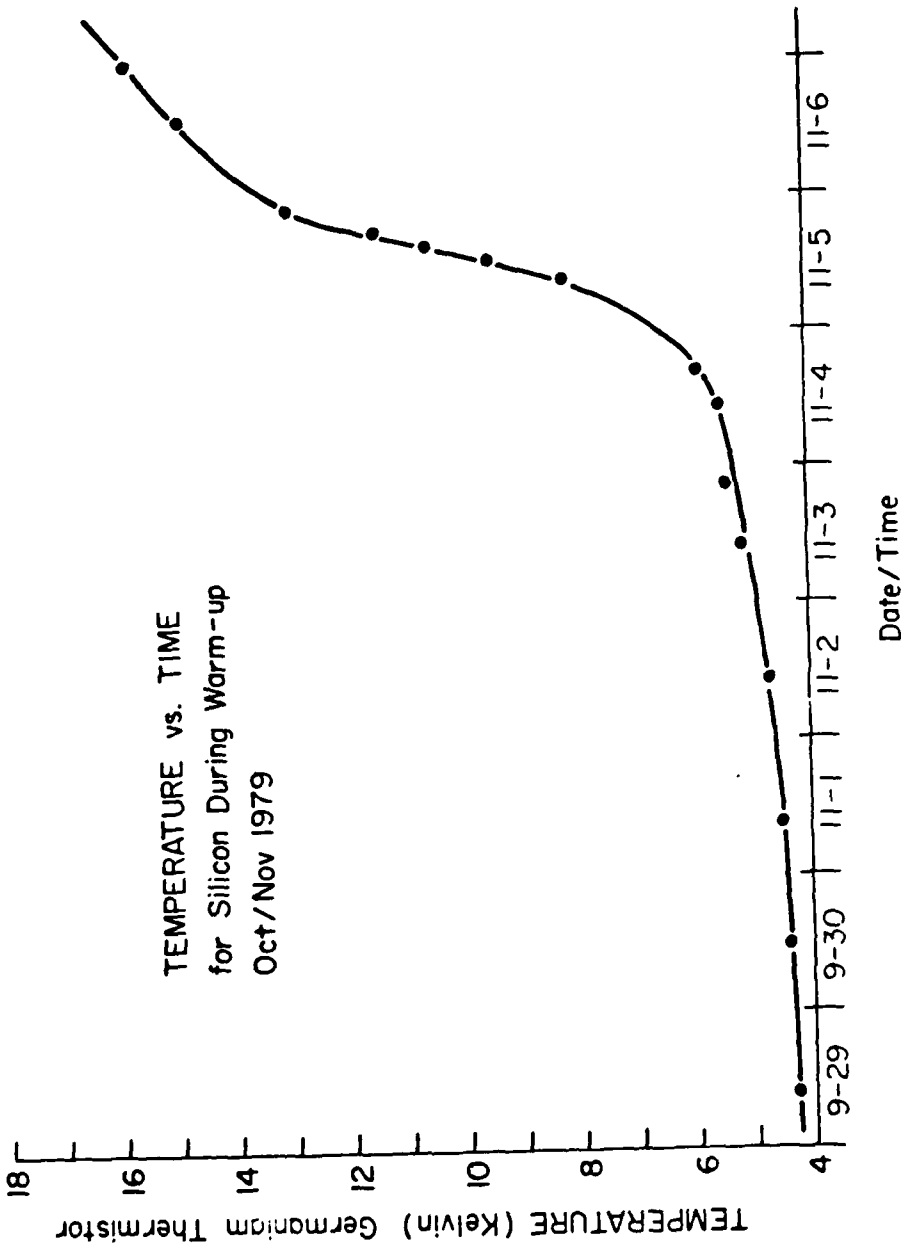
TEMPERATURE vs. TIME
for Silicon During Warm-up
Oct/Nov 1979
TEMPERATURE (Kelvin) Germanium Thermistor
18
16
14
12
10
8
6
4
9-29
9-30
11-1
11-2
11-3
11-4
11-5
11-6
Date/Time

Figure 5.

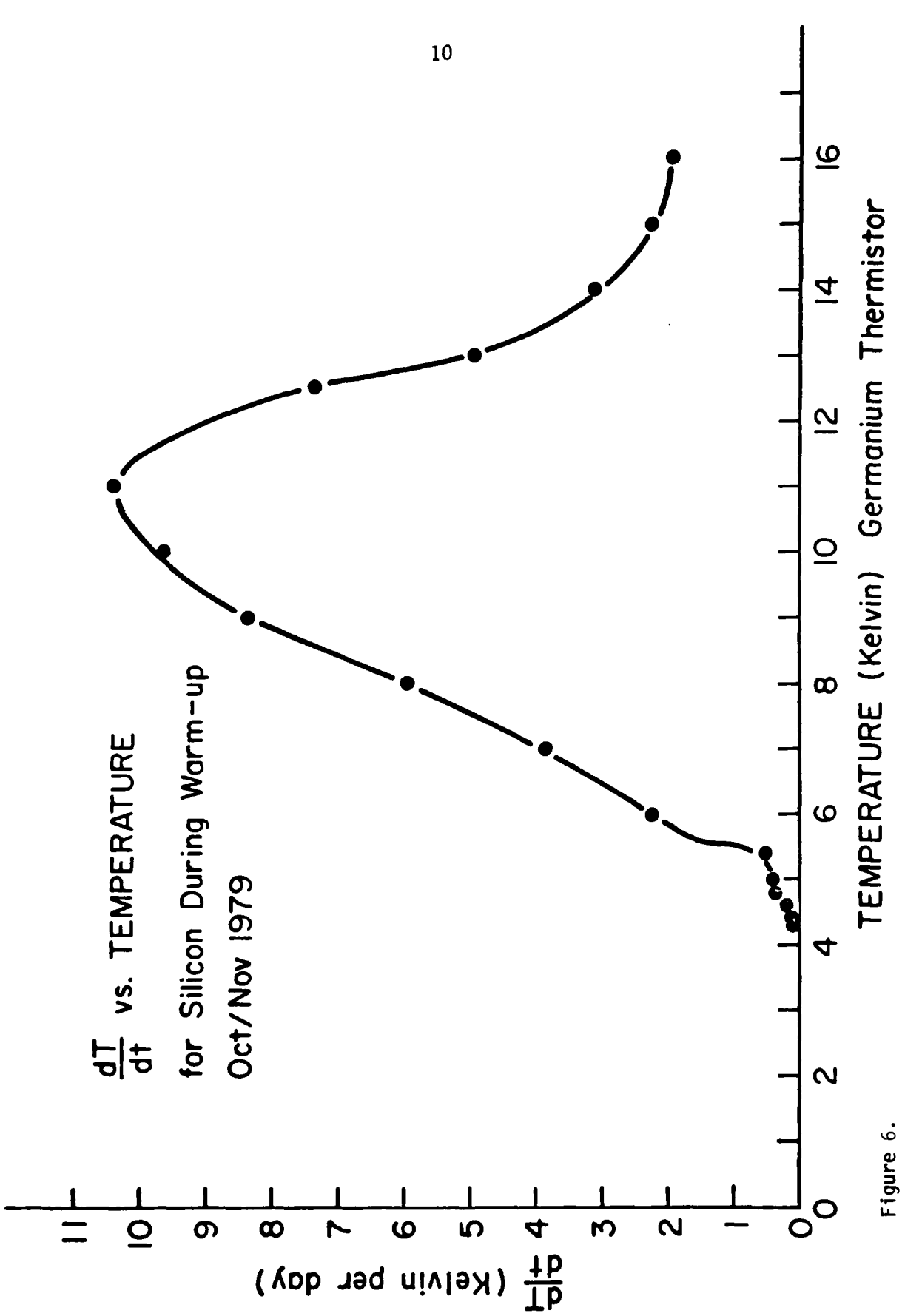
dT/dt vs. TEMPERATURE
for Silicon During Warm-up
Oct/Nov 1979
dT/dt (Kelvin per day)
0
1
2
3
4
5
6
7
8
9
10
11
0
2
4
6
8
10
12
14
16
TEMPERATURE (Kelvin) Germanium Thermistor

Figure 6.

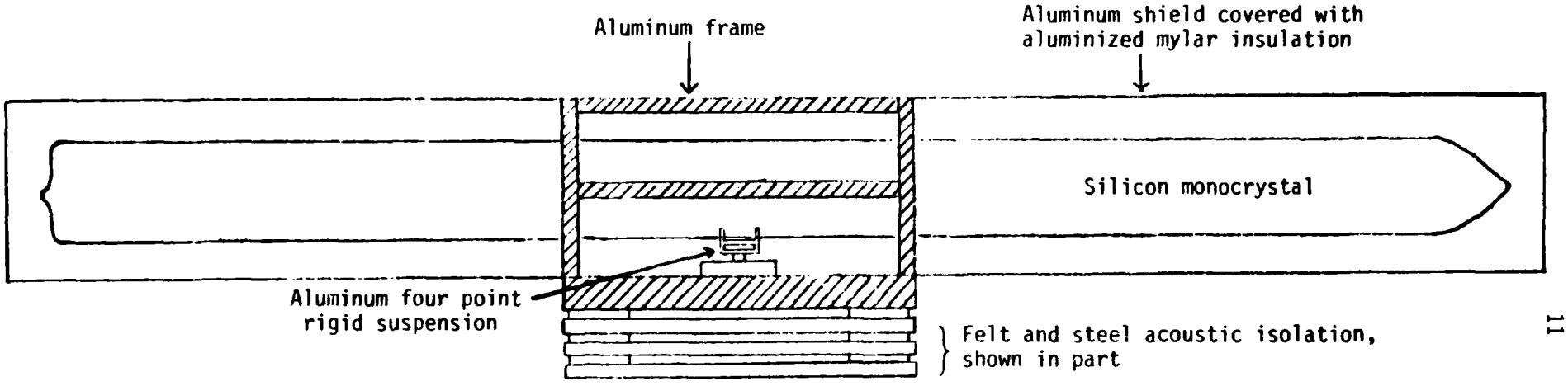

Figure 7. Thermal shield for temperature control of silicon.

crystal and frame is surrounded with an aluminum shield covered with multilayer "superinsulation" (aluminized mylar and nylon netting). Heat conduction into the crystal will take place essentially only from the frame through the suspension. The frame will be actively temperature controlled. This new experiment will include a new carbon glass temperature sensor which has been calibrated at many points. It will be used to more accurately calibrate the previously used germanium and platinum sensors as well as controlling the temperature.

Q measurements up to 280 K are shown in figure 8. There are several gaps in the data which need to be filled. Also it was noted at 27 and 18 Kelvin that the Q is amplitude dependent. Four measurements made at 27 Kelvin are given in table I. For a factor of six smaller amplitude the Q's were 1.6 and 1.3 times higher. Observations of the amplitude dependence of the Q was not attempted at any other temperatures. This behavior can be investigated more closely in the next experiment. Plots of Q as a function of temperature will have to be made with measurements at the same amplitude level or at a level which the Q is not amplitude dependent.

The research group at the University of Rochester under the direction of D. H. Douglass has published measurements of the Q of a silicon crystal as a function of temperature.* Table II compares data on the Maryland and Rochester crystals. The Rochester group has done experiments with other silicon crystals but to this author's knowledge has not yet published the results. The published results show miniumi in the Q curve at 13 and 120 Kelvin. There is no statement of the use of temperature control.

* McGuigan, D. F., Lam, C. C., Gram, R. Q., Hoffman, A. W., Douglass, D. H., and Gutche, H. W., "Measurements of the Mechanical Q of single-Crystal Silicon at Low Temperatures," J. of Low Temp. Phys., 30, 621 (1978).

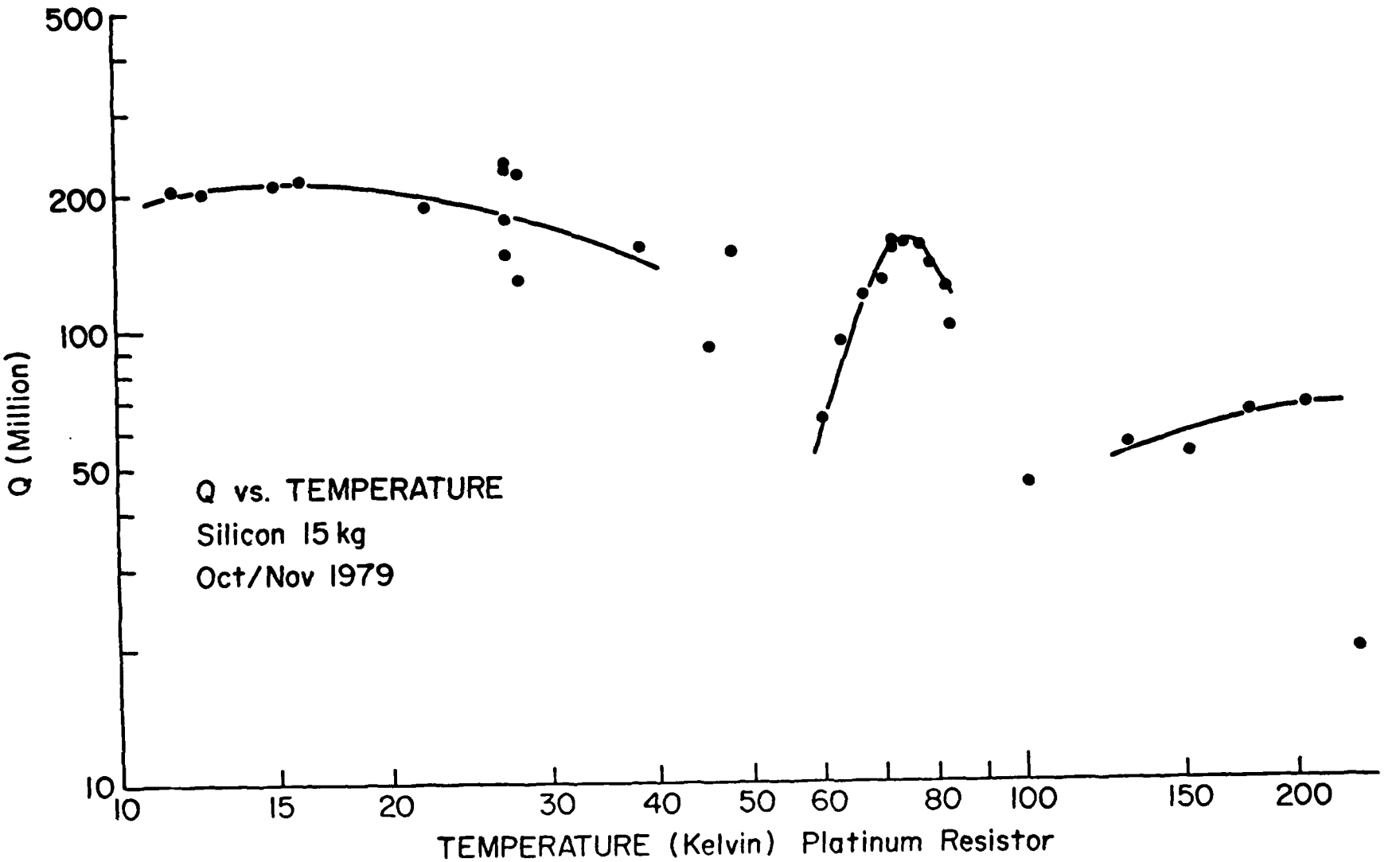
500
200
100
50
10
Q (Million)
Q vs. TEMPERATURE
Silicon 15 kg
Oct/Nov 1979
10
15
20
30
40
50
60
80
100
150
200
TEMPERATURE (Kelvin) Platinum Resistor

Figure 8.

Table I. Amplitude dependent Q measurements made at 27 Kelvin, measurements are in the order in which they were made.

	Frequency (Hz)	Q (10^6)	Starting Amplitude (μv at preamp input)
1.	3467.8186	146	47
2.	3467.8188	228	7.7
3.	3467.8194	174	43
4.	3467.8183	225	7.7

Table II. Comparison of Silicon Crystals used by Maryland and Rochester. Both are boron doped p-type produced by Czochralski process by Monsanto, Inc.

	Maryland	Rochester
Mass (kg)	15.5	4.9
Length (cm)	135	22.9
Diameter (cm)	7.8	10.6
Frequency of fundamental mode (Hz @ <20 K)	3467.8	19553
Density of boron atoms (atoms/cm^3)	8×10^{14}	$2.7 - 4.5 \times 10^{15}$
Surface finish	unfinished	ends cut and polished
Suspension	aluminum four point rigid suspension	tungsten wire
Transducer	Piezoelectric ceramic	DC biased capacitor
Q (4 Kelvin)	2.8×10^{8}	2×10^{9}

Figures 9 and 10 show frequency as a function of temperature for the silicon crystal. The dependence of frequency on temperature below 13 Kelvin is unexpected. The frequency decreases from 13 Kelvin to 4.4 Kelvin by 2.5 ppm. This contrasts with the results of the Rochester group. Their frequency increased by about .25 ppm from 13 Kelvin to 4 Kelvin. It is not clear what caused these differences in data. Conceivably the different suspensions and different transducers might play a part. However, a piezoelectric transducer and four point suspension were also used on the sapphire crystal to be discussed later. From 15 K to 4.5 K its frequency increased by .2 ppm, similar to the Rochester silicon. The sapphire fundamental mode is at 18,642 Hz. This suggests that the suspension and transducer do not produce the relatively large decrease in the fundamental mode of the Maryland silicon below 13 K. This will be investigated further in the upcoming experiment.

Noise of Silicon

A successful measurement of the signal coupling, β, was made for silicon during the experiment. Table III and IV show calculations based on this result. Unfortunately the coupling is too small for practical noise measurements at 4 to 5 Kelvin. Figure 11 gives the expected input noise spectral density to the preamp as a function of frequency. The total noise is due to the preamp itself plus the noise of the crystal. With the narrowest of filters the mean square crystal noise is one part in six of the total mean square noise. This is an unfavorable "signal" to noise ratio. Separate measurements of the mean square total noise and preamp wide band noise can be made simultaneously at two different frequencies. If the wideband pre-preamp noise is assumed to be the same in both bandwidths, then the mean

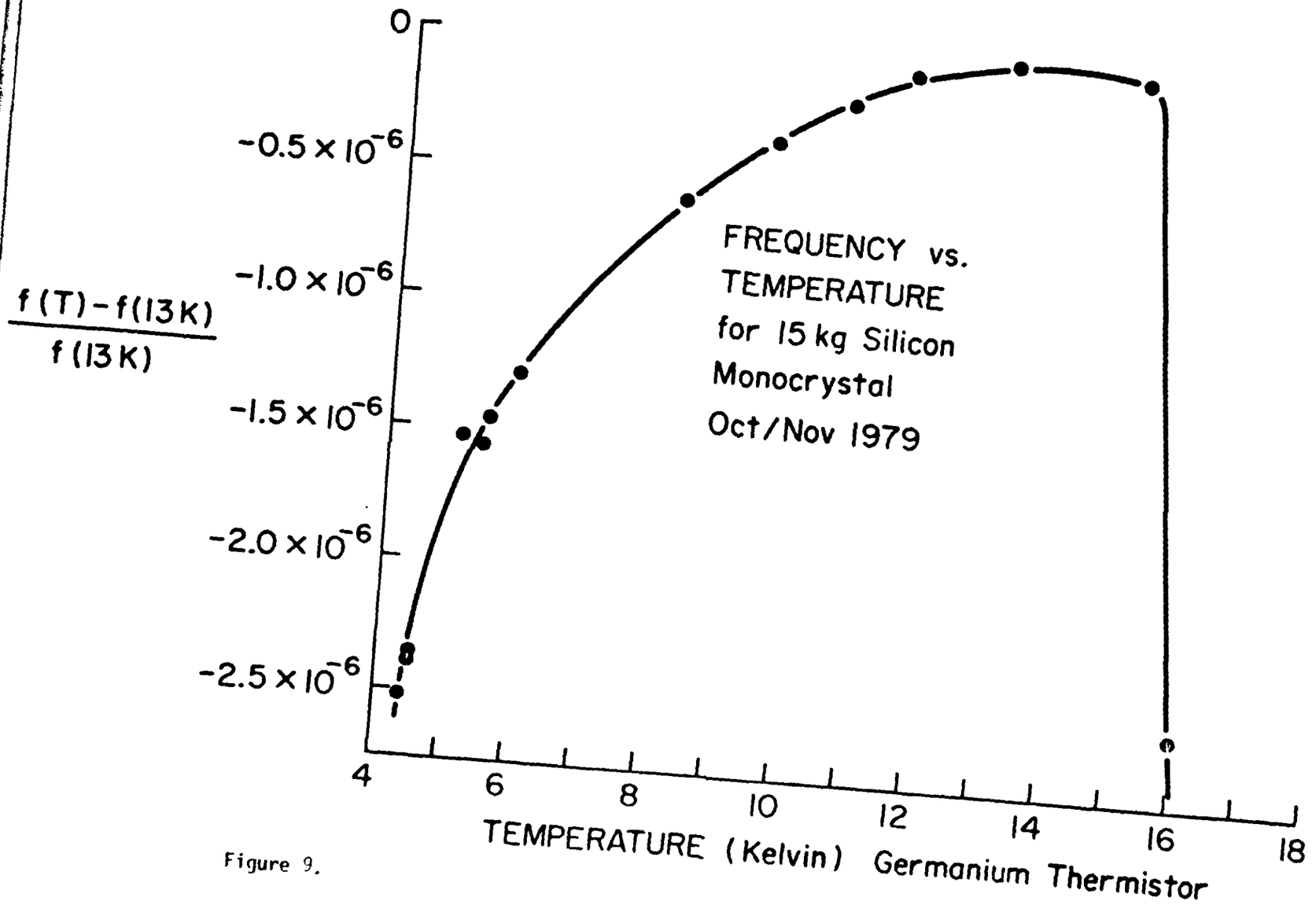
0
-0.5 x 10^-6
-1.0 x 10^-6
-1.5 x 10^-6
-2.0 x 10^-6
-2.5 x 10^-6
f(T) - f(13K) / f(13K)
FREQUENCY vs. TEMPERATURE for 15 kg Silicon Monocrystal Oct/Nov 1979
4
6
8
10
12
14
16
18
TEMPERATURE (Kelvin) Germanium Thermistor

Figure 9.

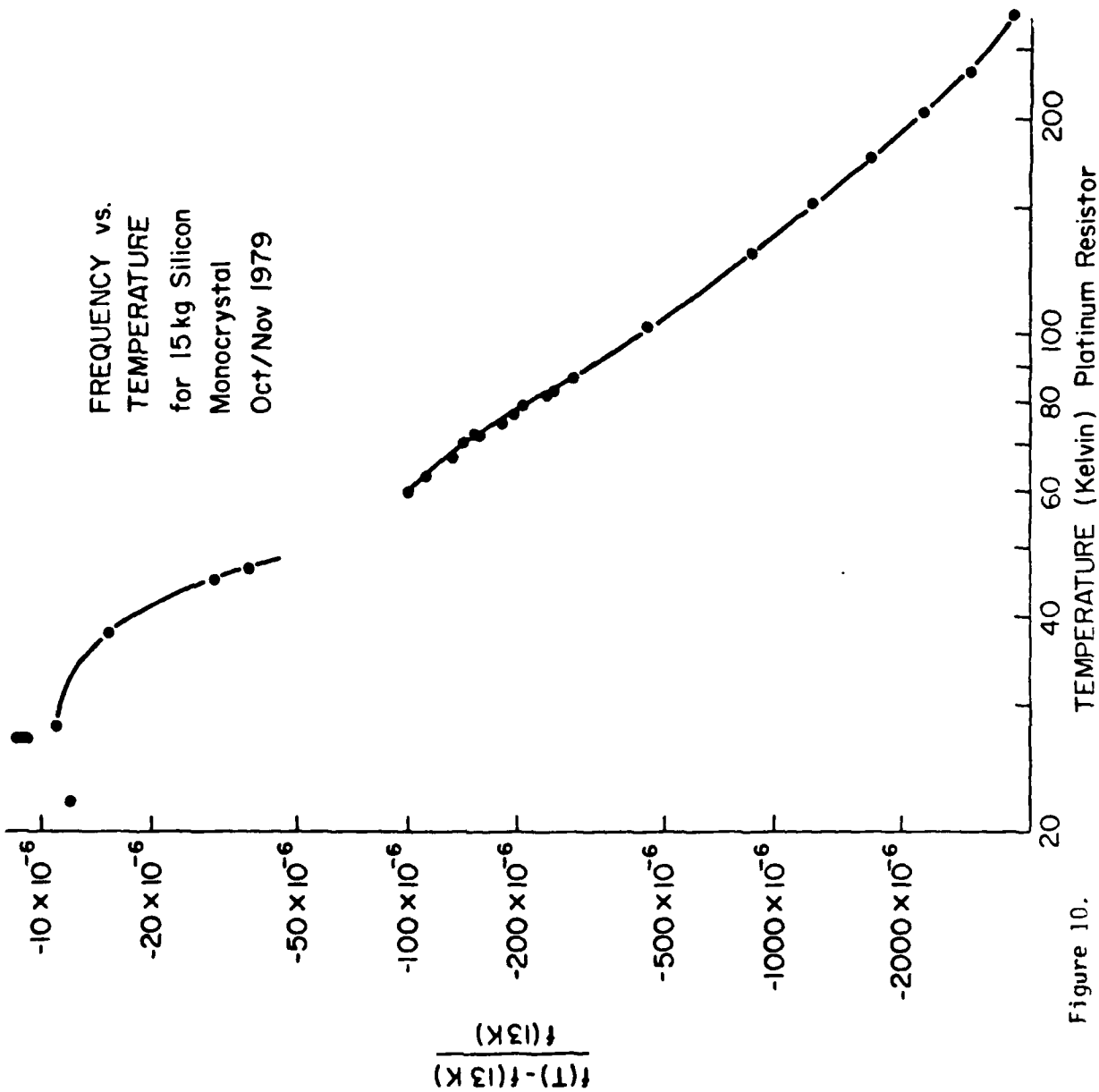
FREQUENCY vs.
TEMPERATURE
for 15 kg Silicon
Monocrystal
Oct/Nov 1979
-10 × 10⁻⁶
-20 × 10⁻⁶
-50 × 10⁻⁶
-100 × 10⁻⁶
-200 × 10⁻⁶
-500 × 10⁻⁶
-1000 × 10⁻⁶
-2000 × 10⁻⁶
f(T) - f(13 K) / f(13 K)
20
40
60
80
100
200
TEMPERATURE (Kelvin) Platinum Resistor

Figure 10.

TABLE III

PROPERTIES OF MONOCRYSTALS COUPLED TO TRANSDUCERS

Data From September 1979 Cooldown

material	mass (kg)	length (cm)	fundamental mode frequency at 4 to 5 Kelvin (hz)	loaded Q at 4 to 5 Kelvin	β at 4 to 5 Kelvin
Silicon	15½	135	3467.8	250×10^{6}	$.17 \times 10^{-9}$
Sapphire	5.2	25	18,642	58×10^{6}	61×10^{-9}

	τ_o (sec)	L_1 (henries)	$R_1 + R_2$ (ohms)	C_1 (farads)	C_2 (farads)	$\frac{\beta k T_n}{C_2}$ (volts)^2
Silicon	23,300	22.2×10^{9}	1.9×10^{6}	95×10^{-21}	550×10^{-12}	$(4.2 \times 10^{-12})^2$
Sapphire	990	1.5×10^{6}	3000	49×10^{-18}	800×10^{-12}	$(88 \times 10^{-12})^2$

TABLE IV

FET NOISE

FET	Voltage noise $e(\nu)$ $(v/\sqrt{hz})$	Current noise $j(\nu)$ $(a/\sqrt{hz})$	FET noise temperature $\frac{e(\nu)j(\nu)}{2k}$ (Kelvin)	FET noise impedance $Z_n = e(\nu)/j(\nu)$ (ohms)	$\frac{1}{\omega Z_n}$ Silicon (farads)	$\frac{1}{\omega Z_n}$ Sapphire (farads)
BF817	1.8×10^{-9}	4.0×10^{-15}	.26	450,000	100	19
CP640	$.70 \times 10^{-9}$	55×10^{-15}	1.4	12,700	3,600	672

FET	$\Delta T = \frac{j^2(\nu)BQ}{4k\omega C_2}$ change in crystal noise temperature due to current noise		$\sqrt{e^2(\nu) + j^2(\nu)\frac{1}{\omega^2 C_2^2}}$ Total wideband noise	
	Silicon (Kelvin)	Sapphire (Kelvin)	Silicon $(v/\sqrt{hz})$	Sapphire $(v/\sqrt{hz})$
BF817	.001	.011	1.8×10^{-9}	1.8×10^{-9}
CP640	.2	2.09	4.7×10^{-9}	$.92 \times 10^{-9}$

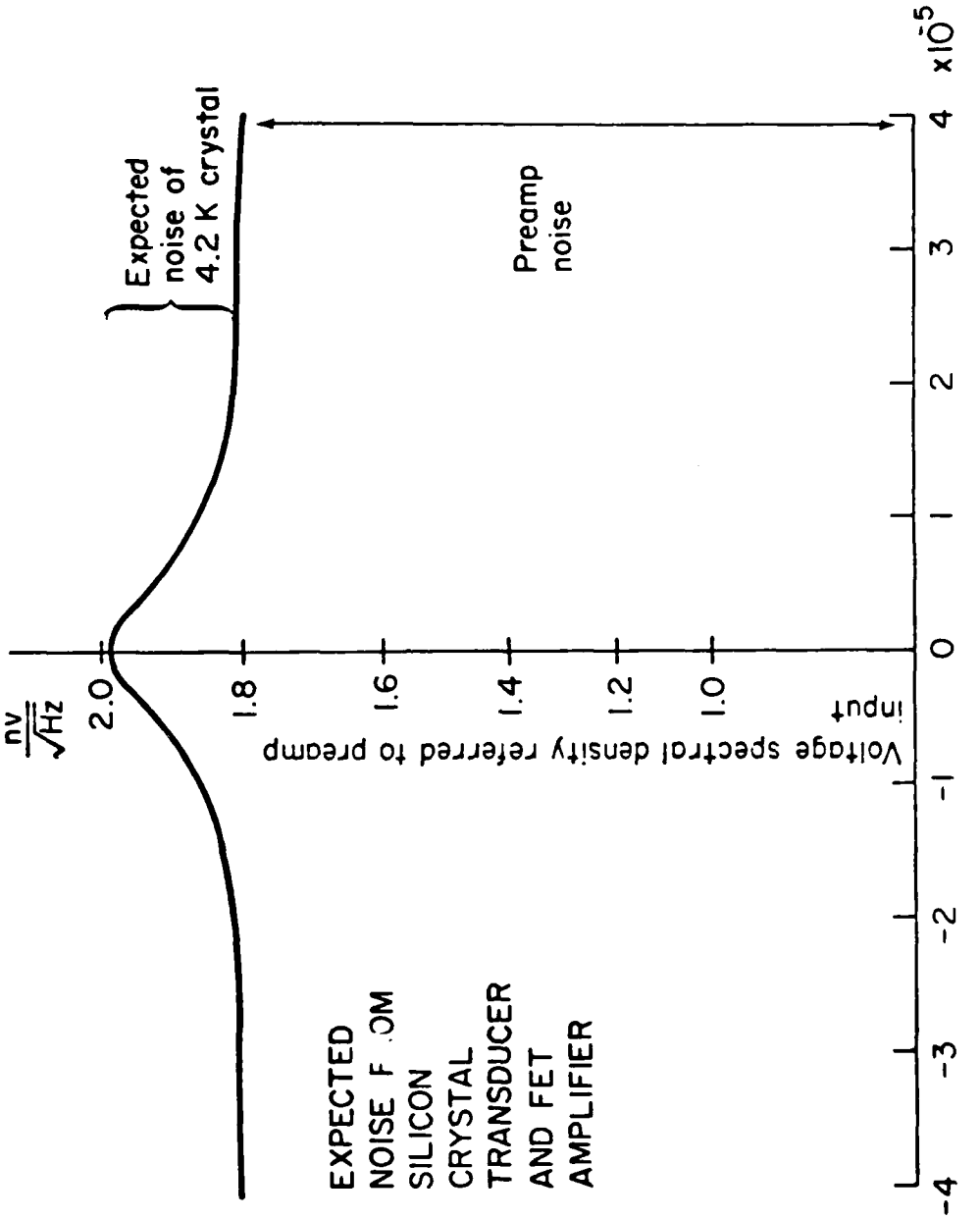

Figure 11. Frequency relative to Silicon mode frequency (Hz)

square wideband preamp noise can be substracted from the total mean square noise to obtain a value for the mean square crystal noise. Unfortunately in order to get enough data for a statistically significant result with this method, the experiment would have to be run for several months. This is not presently practical.

For a given preamplifier and crystal frequency, Q, and temperature, one can choose practical values for the coupling, transducer output impedance, and filtering time constant which tend to maximize the crystal noise with respect to the preamp noise. For the present silicon and FET amplifier these are, $\beta = 6 \times 10^{-8}$, $C_2 = 10^{-10}$ f, and $\tau = 2000$ sec. This produces a peak crystal noise of about 400 times that of wideband contribution of the preamp. A measurement of the noise temperature of the crystal can be made with an uncertainty of about 15% in one day. The above value of β is about 350 times larger than the present value with the piezoelectric transducer. It is not now believed possible to achieve the higher value of coupling with the present transducer without substantually degrading the Q of the crystal. If the ends of the silicon are cut, polished and coated with a metal, then a capacitor transducer and FET preamp can be used to obtain the above β and C_2. If coated with a superconductor then flat superconducting coils with a persistent current and SQUID amplifier can be used to get even better performance. The latter is shown in figure 12. These alternatives are being considered.

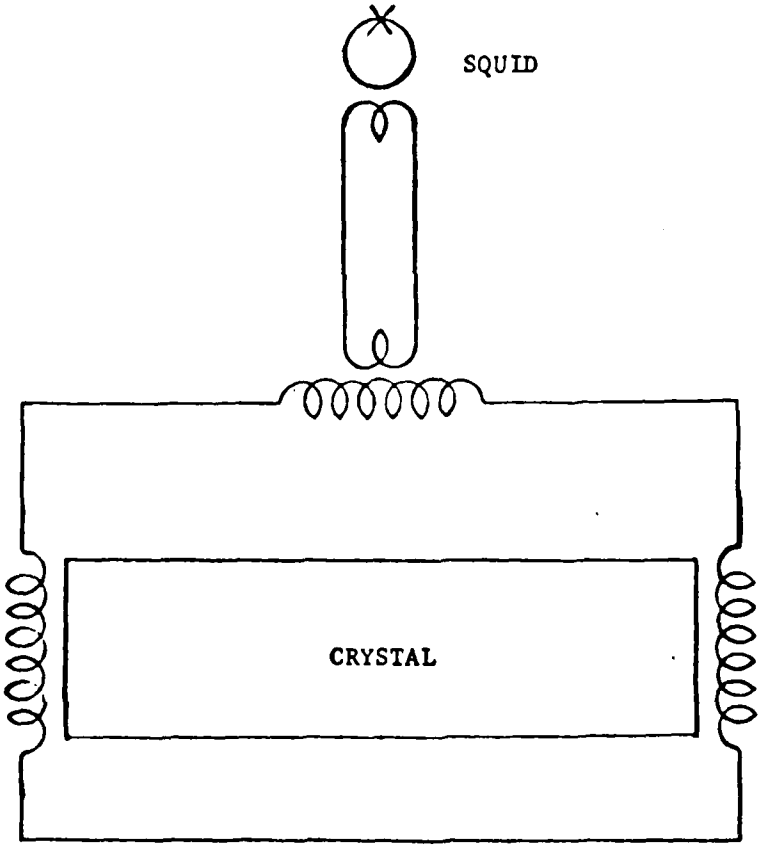

Figure 12. **SUPERCONDUCTING INDUCTIVE PICKUP**

Noise of Sapphire

Noise measurements of the sapphire crystal were obtained when it was at 4 to 5 Kelvin. The results varied from 10^3 to over 10^6 Kelvin instead of the hoped for 6 to 7 Kelvin (thermal temperature plus current noise temperature). There was a strong correlation between this noise and the operation of the helium recovery compressor and the diffusion pump. Also pushing the end of the vacuum chamber produced no audible sound, but the sapphire was clearly excited. Furthermore, by observing the signal from the transducer at low frequencies, pulses were seen when the chamber is pushed, which were interpreted as the rocking of the crystal on its four point suspension. Figure 13 shows a drawing of this suspension. After the experiment was warmed up and the vacuum chamber opened, it was discovered that the crystal had rolled on its suspension as shown in figure 14. Before the cooldown the wires going to the transducer had plenty of slack. As a result of the rolling the wires became taut. At room temperature when the vacuum chamber was pushed, the signal coming from the sapphire was the same as at liquid helium temperatures. When the crystal was rotated back so that the wires were slack again, this behavior stopped. It was concluded that the excess noise observed at liquid helium temperature was due to low frequency vibrations coming through the isolation stacks, and then rocking the crystal on its mount as a result of the tight wires. This then excited the modes of the crystal. Why did the crystal rotate in the first place? If the friction between the mount and the crystal was significantly different for one direction of rotation than for the other, then varying mechanical stresses between the two could produce a net rotation in one direction. Such stresses could arise during cooling or could have been produced by pushing on the vacuum chamber. The crystal sat on sharp

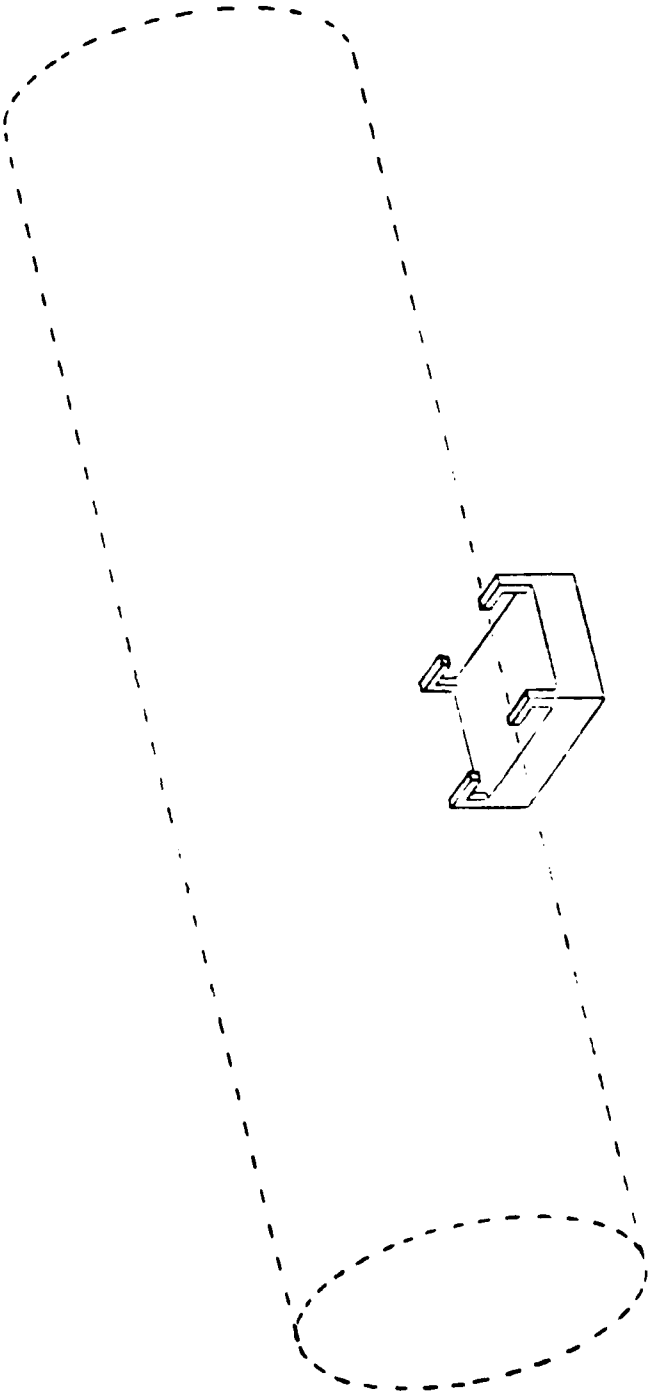

Figure 13. Four point rigid suspension

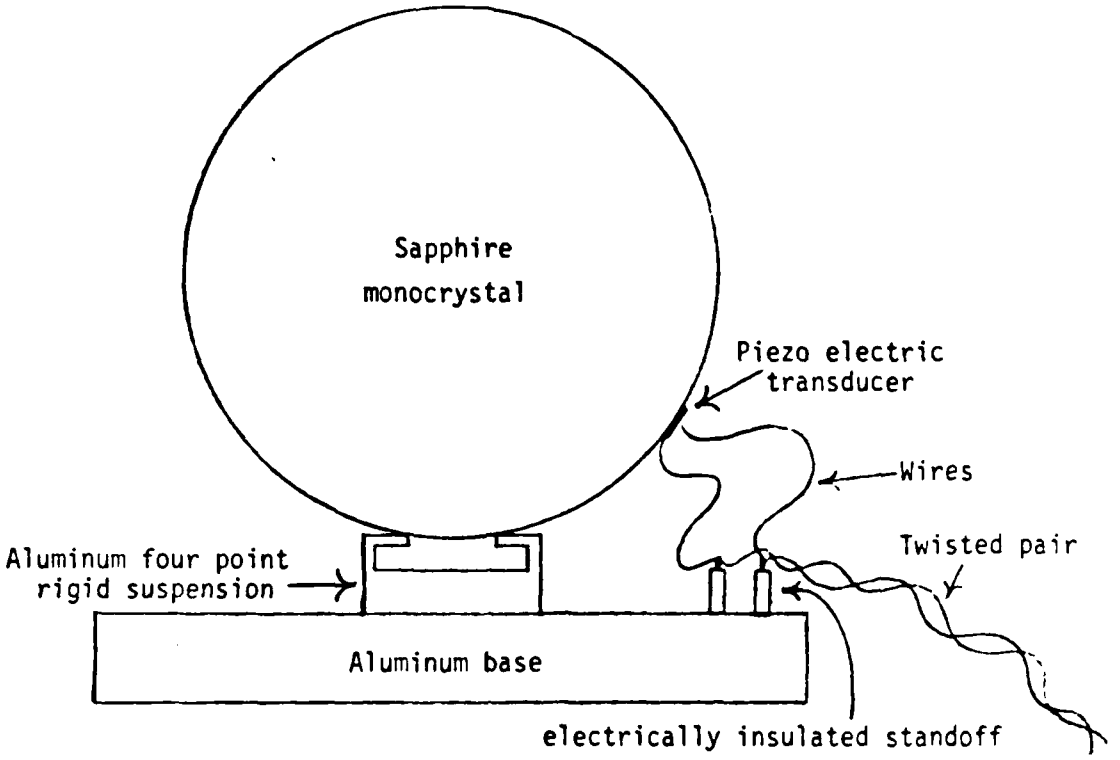

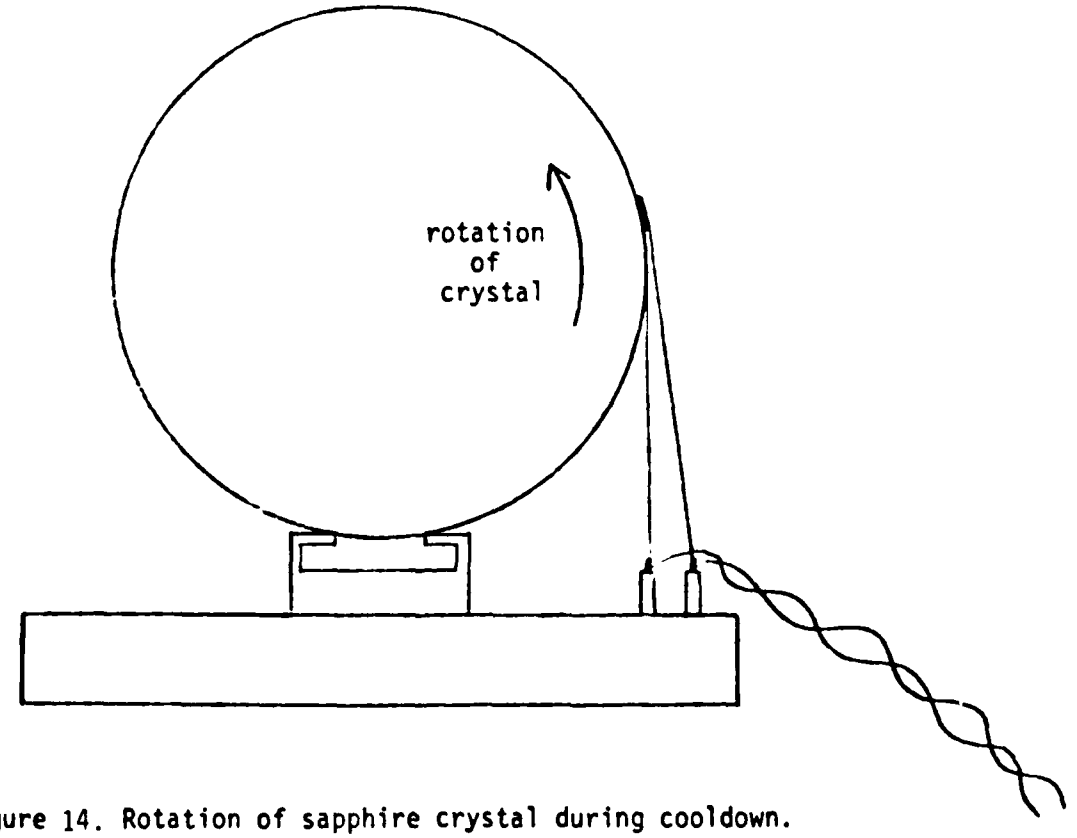

Figure 14. Rotation of sapphire crystal during cooldown.

edges of the four point suspension. If these edges were not identical, then this might produce the differential friction. Future suspensions for the sapphire will have the edges filed to be more nearly identical. If this does not work then we may have to give up the piezoelectric transducer glued on to the crystal and use capacitor plates which have adjustable spacing. In this case movement of the crystal on the mount would not be important as long as the spacing between the capacitor transducer and the end of the bar is adjustable at cryogenic temperatures.

Future Goals

The following is a list of objectives to further cryogenic research of crystals.

1) Q and frequency measurements of silicon with temperature control.
2) Cutting, polishing, and plating the ends of the silicon for use with capacitor transducer and FET amplifier or with flat coil transducer and SQUID amplifier.
3) Noise measurements of silicon in (2).
4) Further noise measurements of sapphire.
5) Assembly and testing of improved electronics. (see figure 15)

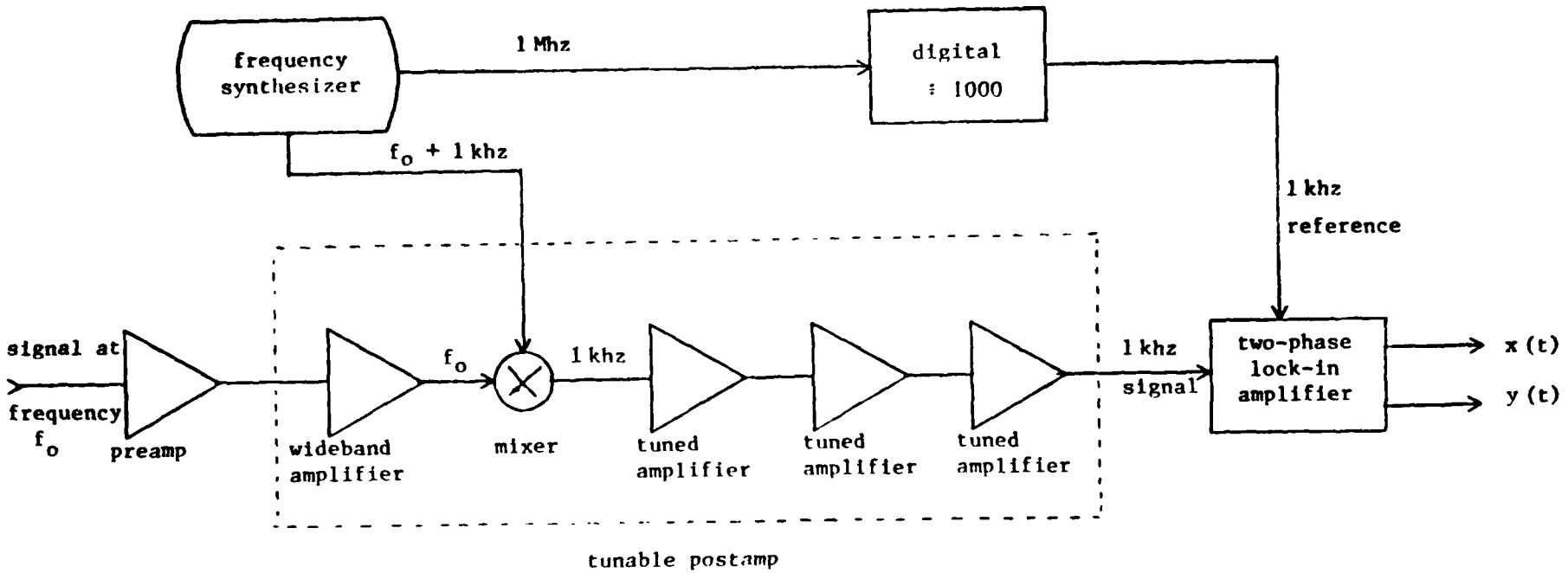

Advantages of system:

1) postamp easily tunable
2) reference frequencies are not at signal frequency
3) postamp bandwidth can be made very small with crystal filters

FIGURE 15. Improved Electronics with Tunable Postamplifier

Observation of well behaved noise and fluctuations in an aluminum cylinder at liquid helium temperatures*

Wm. S. Davis and J.-P. Richard

University of Maryland
College Park, Maryland 20742

June 10, 1980

*A slightly modified form of this paper has been accepted for publication by the Physical Review.

ABSTRACT

A 134 kg aluminum cylinder instrumented with a resonant capacitive sensor and mounted on a new multistage suspension system has been tested. Well behaved thermal noise and fluctuations have been observed. The system fluctuation temperature was 0.51 K, in close agreement with the predicted value.

I. INTRODUCTION

The most obvious application for a cryogenically cooled solid with low normal mode noise is for gravitational gradiometry at high frequencies.

It is therefore most useful to analyze the data in the terms employed for gravitational radiation antennas.

Three approaches have been considered for the detection of gravitational wave emitted in astrophysical events: the Weber type cylindrical resonant antenna,[1] laser ranging between two inertial masses at laboratory distances,[2-5] and doppler ranging to interplanetary probes.[6,7] At present it is not clear which of these methods will prevail. In this paper, we will be concerned specifically with the development of Weber type antennas. Various materials have been considered for such antennas. Aluminum or niobium are materials with moderately high mechanical quality factor. With these, large masses can be obtained. Monocrystalline material such as grown silicon[8,9] or sapphire[10] have higher Q factor. Masses of the order of 30 kg can presently be obtained. The sensitivity of a Weber type antenna is a function of Q, mass and temperature. It is useful to investigate these materials and study their thermal noise behavior at cryogenic temperatures. This paper reports on the observation of well behaved thermal noise and fluctuations in a 134 kg aluminum cylindrical antenna resonant at 1754.9 Hz and cooled to liquid helium temperature. A new sensor and suspension system were used for this experiment. In section II, quantities related to the experiment are defined. In section III to V, the system which has been tested is described and in section VI, the method of data taking and analysis is given. The results are presented and discussed in section VII.

II. ANTENNA SENSITIVITY

Many discussions on the sensitivity of a Weber type resonant antenna have been presented before.[10-25] A convenient expression for the detection of short pulses of gravitational radiation is:

$$F(f) \geq \frac{\pi c^3 k_B}{8G v_s^2} \left(\frac{T_p}{M}\right) \ln (1/\tau R) \qquad (1)$$

where F(f) is the required incident energy spectral density for detection. c is the speed of light, k_B, the Boltzmann constant, G, the gravitational constant and v_s, the speed of sound in the antenna material. T_p is the effective noise temperature of the system for the detection of pulses shorter than the resolution time τ of the system. M is the mass of the antenna and R is the assumed rate of incoming pulses. T_p is related to the fluctuations in the amplitude of vibration of the cylindrical antenna in its lowest longitudinal mode. $(X + iY)e^{i\omega_a t}$ refers to the displacement in that mode with ω_a being the radial frequency of the antenna. With proper normalization of X and Y, the energy in the fundamental mode of the antenna is $X^2 + Y^2$ and the temperature of the fundamental mode is related to it by

$$k_B T_E = \langle X^2 + Y^2 \rangle \qquad (2)$$

x and y are phase sensitive detected and filtered measures of X and Y. They include noise contributions not related to the state of the antenna. The fluctuations ΔE in the measured state of the antenna and an equivalent fluctuation temperature are defined by

$$k_B T_F = \langle \Delta E \rangle = \langle [(\dot{x})^2 + (\dot{y})^2] \rangle \tau^2 \qquad (3)$$

where τ is equalled to the time constant of the x and y averaging filters. Eq. (3) also assumes proper normalization of x and y. In the experiment reported here, second order butterworth filtering of x and y is used. T_p and T_F are then simply related by:

$$T_p = e^{\pi/2} T_F$$

ΔE as given in eq. (3) is a useful measure of the expected energy in the fundamental mode contributed by the noise sources after a time τ to a system initially at rest. Eq. (1) essentially states that in order to be detected, a short pulse should deposit in the antenna a comparable or larger energy. Special effort was done during the experiment to achieve a very low value for T_F and a proper distribution of the fluctuations as a measure of the potential sensitivity of the detector.

III. THE CRYOGENIC ANTENNA

The antenna-sensor-suspension system used in the experiment is shown on Figure 1. Briefly, the antenna is a 134 kg aluminum cylinder 20 cm in diameter and 150 cm long with a loaded fundamental mode at 1754.9 Hz. It is supported by a four point suspension consisting of a "split ring" as shown in Figure 1 and discussed in ref. 23. This four point suspension rests on a short filter stack of alternate layers of felt and steel. This assembly is supported by two 150 cm long arms which constitute a low frequency "bridge" filter stage. The arms rest at both ends on felt and steel filter stacks which provide additional acoustic isolation. The antenna is instrumented with a dc biased resonant capacitor sensor shown schematically on Figure 2. There, plate P_1 is rigidly attached to the antenna. Plate P_2 is coupled to the antenna through a high Q suspension resonating near the fundamental mode of the antenna. A constant biasing charge is maintained on the capacitance C_3 formed by P_1 and P_2 through a high impedance circuit. Vibrations of the antenna modulate the capacity C_3 resulting in an ac voltage detected with a low noise FET preamplifier. The antenna and P_2 behave as two coupled harmonic oscillators. This system exhibits two modes which in our case are at $\omega_a = 2\pi \times 1754.9$ rad/sec and $\omega_c = 2\pi \times 1801$ rad/sec. The mode at ω_a is the one of interest here because it is dominated by the antenna energy and accordingly is the more strongly coupled to the gravitational field. The frequencies of the modes are selected to achieve large mechanical coupling between the antenna and the sensor while insuring that the observed thermal noise contribution originating in the suspension of the resonating plate is less than the contribution originating in the antenna itself, this in the bandwidth of interest centered on the antenna mode.[22] The mass m_2 of the resonant plate and the biasing charge on

the capacitor are selected to achieve desired coupling between the mechanical system and the electronics. The antenna sensor system has been tested at room temperatures and the predicted thermal noise level has been observed for values of the bias voltage up to 800 v corresponding to field intensity between the plates of 1.6×10^7 v/m.[23]

IV. THE CRYOGENIC SYSTEM

The cryogenic installation used in the experiment consists essentially of a CTI model 1400 helium liquefier, associated compressor and recovery tank for helium gas, and a cryostat. The cryostat has a cylindrical test chamber 1.7 m long and 50 cm in diameter. For the experiment, the antenna and its suspension as shown on Figure 1 are mounted inside the test chamber. The chamber is enclosed by a double wall stainless steel cylinder. The space in this wall forms a liquid helium dewar with a storage capacity of 120 liters. The dewar is surrounded by a helium gas cooled shell operating near 55 K. Multilayer insulation surrounds the helium dewar and the gas cooled shell to reduce radiation heat leaks. A vacuum near 10^{-6} torr is maintained in the vacuum chamber to keep heat conduction losses through residual gas at a low level. The test chamber is sealed from the rest of the cryostat so that helium pressure near 10^{-3} torr can be maintained to accelerate cooling of the antenna and help maintain thermal equilibrium between the antenna and the surrounding liquid helium dewar.

The procedure used has been to liquefy helium gas and fill the liquid helium dewar. The liquefier operation is then stopped. One compressor is used to return the helium gas boiled off to the recovery tank. The boiloff rate is 15 liters/day so that an experiment can last 7 days without liquefier operation. If useful, the liquefier can be restarted after 7 days to continue the experiment. The 134 kg aluminum antenna can be cooled to 4.2 K in 6 days.

V. PREDICTED FLUCTUATIONS

Figure 3 shows the ac equivalent circuit of the system including the antenna, the sensor, and the preamplifier in the vicinity of the antenna mode ($|f-f_a|<<60$ Hz). There, L_a, C_a, R_a and $e_a(f)$ represent the mass, the stiffness, the losses and the thermal noise in the antenna. $i(f)$ and $e(f)$ are current and voltage noise sources describing the noise contribution of the sensor and the amplifier. C_T equals the sensor capacitance C_3 plus stray capacitances. $\beta = C_a/C_T$ is the energy coupling. $\beta<<1$ is assumed. The calculated fluctuations in the observed bandwidth due to $e_a(f)$, $i(f)$ and $e(f)$ are:

$$k_B T_F = <\Delta E> = \frac{k_B T_a \tau}{\sqrt{2}\,\tau_a} + k_B T_e \left[\frac{\lambda + \lambda^{-1}}{\sqrt{2}\,\beta\tau\omega_a} + \frac{\beta\tau\omega_a}{4\sqrt{2}\,\lambda} \right] \qquad (5)$$

τ_a is the damping time of the antenna. It is related to its mechanical Q by $\tau_a = 2Q_a/\omega_a$. $\tau<<\tau_a$ is assumed. T_e is the noise temperature of the preamplifier defined by:

$$2k_B T_e = e(f)\, i(f)\,. \qquad (6a)$$

Also:

$$\lambda = Z_{op}/|Z| \qquad (6b)$$

$$Z_{op} = e(f)/i(f) \qquad (6c)$$

$$Z = (\omega_a C_T)^{-1} \qquad (6d)$$

The first term is the noise induced in the antenna by thermal noise originating in the antenna. The second term is the wide band noise contributed by the sensor and the amplifier. The third term is noise induced in the antenna by the sensor and the amplifier. It was experimentally determined that $\beta Q_a = 2000$ can be obtained with the present sensor at 4.2 K. However, such

a high βQ_a was not required here for the minimization of T_F[23]. The values of τ, λ and β were selected to achieve a low value of T_F. The preamplifier following the sensor used a low noise BF 817 field effect transistor. The selected transistor had a voltage noise density $e(f) = 1.8 \times 10^{-9} v/\sqrt{Hz}$ and a current noise density $i(f) = 4 \times 10^{-15} A/\sqrt{Hz}$ corresponding to a noise temperature of 0.26 K [Eq. (6a)]. In the present case, Z_{op} as given in Eq. (6c) is 450 kΩ. The impedance of the resonant capacitor and coaxial lines at 1754.9 Hz is ∿195 kΩ, thus giving a value for $\lambda = 2.3$. The following values also apply: $\beta Q_a = 36.6$, $\beta = 3.75 \times 10^{-5}$, $\tau_a = 177$ sec and $\tau = 12$ sec. For $T_a = 4.2$ K, Eq. (5) predicts an equivalent mean fluctuation in the observed bandwidth of 0.40 K. This assumes that the contribution from the sensor to the current noise i(f) is negligible, an assumption confirmed by independent measurements of the white noise in the system.

Additional Instrumentation

The following is a brief description of additional electronics used in this experiment. The capacitor sensor is biased with dry cell batteries through a two stage RC filter with a time constant of approximately five minutes. The ac signal generated by the antenna across the capacitor sensor passes through a dc blocking capacitor to the room temperature electronics shown on Figure 4. The electronics generate voltages in the x and y channels which are the in phase and quadrature components of the signal with respect to a reference frequency appropriately close (as specified later) to the antenna frequency. The preamp is a tuned cascode with the BF 817 previously specified at its input. The preamp has a gain of 250 and a 3-dB bandwidth of 30 Hz. The postamp consits of four cascaded

single-tuned amplifiers with an overall gain of 10^5 and a 3-dB bandwidth of 14 Hz. The averaging filters for x and y have a time constant $\tau_E = 3.5$ sec. The filters and differentiator in the fluctuation channels have the previously specified time constant $\tau = 12$ sec. The outputs were recorded on chart recorders and magnetic tape. On the latter, the resolution was six bits for each channel and the sampling rate was 10 Hz. After the experiment was completed, a computer was used to analyze the data on tape.

VI. SYSTEM EQUIVALENT CIRCUIT

Since the sensor and stray capacitances did not contribute significant electrical noise or losses, e(f) and i(f) as shown on Figure 3 are the noise contributions of the BF 817 preamplifier. The 25 MΩ resistor shown was used as a calibrated reference noise source through its own 300 K thermal noise. A measurement of L_a was made by measuring the decay time τ_a of the antenna as a function of the value of an external resistor placed at the preamplifier input. The external resistor R_e adds to the dissipation of the antenna and if R_e satisfies $R_e >> 1/\omega_a C_T$, it does not alter in a significant way the characteristics of the equivalent circuit. By plotting τ_a^{-1} versus R_e, a straight line with a slope $(2L_a)^{-1}$ was obtained which gave L_a $(4.7 \pm 0.3) \times 10^5$ h. L_a was also calculated from theory using the following relations:

$$L_a = \frac{m_2}{(V_B C_3/s)^2} \left(\frac{\omega_2^2}{\omega_a^2} \right) \left(\frac{\omega_c^2 - \omega_a^2}{\omega_1^2 - \omega_a^2} \right) \tag{7}$$

where m_2 is the mass of the resonating plate and s is the spacing between the capacitor plates. The uncoupled antenna (ω_1) and transducer (ω_2) resonant frequencies are calculated from:

$$\omega_1^2 = \frac{1}{2} \left[\omega_a^2 + \omega_c^2 - \left((\omega_c^2 - \omega_a^2)^2 - 4\omega_a^2 \omega_c^2 (m_2/m_1) \right)^{\frac{1}{2}} \right] \tag{8}$$

and

$$\omega_2 = \omega_c \omega_a / \omega_1 \tag{9}$$

The other parameters are: $m_1 = 67$ kg, $m_2 = 0.039$ kg, $s = 50 \times 10^{-6}$ m, and $C_3 = 406 \times 10^{-12}$ f. For the noise measurements reported here the bias voltage, V_B, was set at 63 volts. The value of L_a obtained from eqs. (7-9) was $(4.9 \pm 0.4) \times 10^5$ h. It is consistent with the decay time determination. The latter was used to compute C_a and $\beta = (3.75 \pm 0.2) \times 10^{-5}$. The related quantities shown on Figure 5 were derived from these and from a measurement of the decay time: $\tau_a = 177 \pm 3$ sec.

With the filtering shown on Figure 4 and used in the experiment, the average measured energy is predicted to be:

$$\langle x^2 + y^2 \rangle = k_B T_a + \frac{e_n^2(f) C_T}{\sqrt{8}\, \tau_E\, \beta} + \frac{\beta i^2(f) \tau_a}{8 C_T} \qquad (10a)$$

or

$$\langle x^2 + y^2 \rangle = k_B T_E + \frac{e_n^2(f) C_T}{\sqrt{8}\, \tau_E\, \beta} \qquad (10b)$$

where

$$e_n^2(f) = e^2(f) + i^2(f)/\omega_a^2 C_T^2 \qquad (11)$$

$\tau_E \ll \tau_a$ is assumed. The average fluctuation follows from eqs. (5) and (6):

$$\langle \dot{x}^2 + \dot{y}^2 \rangle \tau^2 = \frac{k_B T_a \tau}{\sqrt{2}\, \tau_a} + \frac{e_n^2(f) C_T}{\sqrt{8}\ \tau \beta} \quad \frac{\beta i^2(f) \tau}{8 C_T \sqrt{2}} \qquad (12a)$$

or

$$\langle \dot{x}^2 + \dot{y}^2 \rangle \tau^2 = k_B T_F \qquad (12b)$$

The corresponding predicted outputs of the electronics in volts squared referred to the input of the preamplifier are $(x^2 + y^2)\beta/C_T$ and $(\dot{x}^2 + \dot{y}^2)\tau^2\beta/C_T$. Substituting numerical values in the above equations gives the corresponding expected contributions to T_E and T_F: $T_E = T_a + 2.1$ K. $T_F = .048\ T_a + 0.20$ K.

In order to obtain a calibration of the output of the electronics, the following procedure was used. The reference oscillator was detuned from the antenna mode by about 1.8 Hz, so that the narrow band noise was outside the bandwidths of the lock-in amplifier filters (Δf = .10 Hz for energy measurements and Δf = .03 Hz for fluctuation measurements). In such a case and for calibration purposes, the equivalent circuit reduces to C_T. Then the reference noise source was placed at the preamplifier input. This consisted of the thermal noise of a 25 MΩ metal film resistor in series with a 10^{-11}f silver mica capacitor, both at room temperature (Figure 3). The change in the average output contributed by this network gives a calibration of the output of the electronics as referred to the input of the preamplifier.

If all sources of noise in this experiment are Gaussian distributed then both $x^2 + y^2$ and $(\dot{x}^2 + \dot{y}^2)\tau^2$ are exponentially distributed. Let u be either of these outputs. Let a be the mean value of u. Then the expected probability density for u is $p(u) = a^{-1} \exp(-u/a)$. The log of p(u) versus u is then a straight line of slope $-a^{-1}$. The height distribution of the measurements is proportional to the probability density. By plotting the log of the height distribution of the outputs, the exponential character is verified and the average value is determined.

VII. RESULTS

The specific cryogenic experiment reported in this paper started June 26, 1977. Six days later, on July 2, all the liquid helium had evaporated. While there was liquid helium in the dewar, a gas compressor was kept running to recover the boiloff helium. Magnetic tape recording of the data was started on June 30 and continued until 12 hours after complete boil off of the liquid helium. The observed mode temperature for the 54 hour recording period ranged from 5 to 15 Kelvin. The recovery compressor, helium bubbling, and/or the oil diffusion pump could have contributed mechanically or electrically excess noise to the system. It is not clear, however, which of these sources if any contributed to the excess noise and what the coupling mechanism was.

The measurements of the fluctuation temperature were complicated by an unstable reference oscillator. This was not discovered until July 2. The capacitor which trimmed the frequency ω_R of the reference crystal controlled oscillator was slightly unstable mechanically. An error of tuning leads to fractional fluctuations $\simeq (\omega_R - \omega_a)^2\tau^2$. If this is to be less than the expected fractional thermal fluctuation $= \tau/\tau_a$ then, the following condition must be satisified:

$$\tau_a\tau \quad (\omega_R - \omega_a)^2 \quad << \quad 1 \qquad (14)$$

The tuning required for the mode temperature measurement is less stringent by a factor τ/τ_a. There were three measurements of the fluctuation temperature during which the reference was known to be properly tuned. The fluctuation temperatures during these periods were .71 K, .59 K and .51 K.

A more detailed description of two of the mode temperature measurements and the last of the fluctuation measurements will now be given. For these measurements, the compressor and the diffusion pump were off and there was no

liquid helium left in the cryostat. Figure 5 shows the distribution of the $(x^2 + y^2)$ samples taken when the antenna thermal temperature was 6.6 K. Figure 6 and 7 show the distributions of the samples of $x^2 + y^2$ and $(\dot{x}^2 + \dot{y}^2)\tau^2$ taken simultaneously when the antenna thermal temperature was 8.1 K. The vertical axis is the number of samples obtained corresponding to a given temperature. The horizontal axis is generated from data on the tape by multiplying by the calibration which converts to volts squared at the preamplifier input and then dividing by $k_B\mathcal{E}/C_T$ to obtain temperature. The lines shown are from a linear least squares fit where each point is weighted by its variance, assuming the variance is proportional to the number of samples in each bin of the distribution. The exponential function shows the slope of the fit. In Figures 5 and 6, the slopes correspond to the mode temperature plus wideband noise (eq. (12)). In Figure 7, the slope corresponds to the fluctuation temperature (eq. (13)). All of the data for the periods of time labeled are shown on each graph. There has been no processing other than that described above. The horizontal axis of Figures 5 and 6 cover the entire dynamic range of the six bit recording system. The horizontal axis of Figure 7 shows three quarters of the available dynamic range of the electronics. However, there was no data above $\Delta E/k_B$ = 3.2 Kelvin.

The sampling time (.1 sec) was significantly smaller than the autocorrelation time for the $x^2 + y^2$ measurements (177 sec) and the fluctuation measurements (12 sec). Thus the samples shown in Figures 6 and 7 are not independent but represent all the collected data during the times shown. An estimate of the standard deviation of each point on the graphs can be made. For the $x^2 + y^2$ measurements,

$$\sigma \approx \sqrt{\frac{\tau_a}{.1 \text{ sec}}\ (\text{number of samples})}$$

and for the fluctuation measurements,

$$\sigma \approx \sqrt{\frac{\tau}{.1 \text{ sec}} \text{ (number of samples)}}$$

All the data is consistent with such standard deviations.

The data shown in Figure 6 shows one point significantly higher than the others at 53 Kelvin. This point, however, includes all the samples at 53 Kelvin and above and does not represent an excess above the exponential distribution.

The mode temperature was computed from time averages of the data in the following way. The average wide band noise, measured when the reference oscillator was detuned from the antenna frequency, was substracted from the average noise measured when the reference was tuned. These measurements are summarized in table 1. Three sources of error contributed importantly to the uncertainties listed in this table. Firstly, the errors in the measured parameters of the equivalent circuit result in a 6% uncertainty in β and, correspondingly in the measured noise temperatures. Secondly, errors in the calibration of the electronics contribute a 10% uncertainty to the measured noise temperatures. Finally, there is a random error in the measured mean square value of the noise. This error depends on the length of time covered by the collected data and on the autocorrelation time of that data. For the data shown in the table, this random error contributed uncertainties ranging from 6% to 24%.

The major goal of the experiment was to make noise measurements of an aluminum antenna at liquid helium temperatures with the dc biased resonant capacitor. This goal was achieved and the results agree with theoretical calculations based on the known sources of noise. As a detector of gravitational radiation, the system was limited by Brownian motion of the antenna and the noise of the amplifier and not by the capacitor sensor. Because of its relatively small mass, it was no more sensitive than present room temperature detectors. The expected pulse sensitivity temperature from equation (4) and from the measured fluctuation temperature of T_F = .51 K is T_p = 2.4 Kelvin. If the detector was to be used to observe pulses of gravitational radiation, optimal filtering would have been developed and used for data analysis. Also, the corresponding optimal β would have been selected. In that case, the detector sensitivity would have been limited by the preamp noise, and the expected pulse noise sensitivity would have been near .52 Kelvin.

Conclusion

We have observed well behaved noise and fluctuations in a 134 Kg Weber type gravitational radiation antenna at cryogenic temperatures. The predicted values of thermal and instrumentation noise were observed when exterior sources of noise were removed. We conclude that internal stresses introduced in the antenna by sensor mounting and otherwise very simple four-point suspensions have not prevented the antenna from reaching thermal equilibrium and displaying normally distributed fluctuations within the practically short time of a few days. It is also concluded that a sensitivity significantly better than 0.5 K may be obtained with a resonant capacitor sensor such as used here and lower noise Josephson-Junctions electronics,[28] since $\beta Q_a = 2000$ have been achieved with the present sensor.

Acknowledgements

We would like to acknowledge very useful conversations with G. Pizzella and colleagues and with Ho Jung Paik. We are indebted to M. Lee for computer processing of the data and to D. Gretz and G. Rydbeck for their contributions to the design and development of the cryogenic facilities used in the experiment. We are particularily indebted to J. Weber for enthusiastic encouragement through all phases of the experiment.

REFERENCES

[1] J. Weber, General Relativity and Gravitational Waves (Interscience Publishers, Inc., New York, N. Y., 1961).

[2] G. E. Moss, L. R. Miller, and R. L. Forward, Applied Optics 10, 2495 (1971).

[3] R. Weiss, Quarterly Progress Report, Research Lab of Electronics, M.I.T. 105, 54 (1972).

[4] W. Winkler, in Proceedings of the International Symposium on Experimental Gravitation, Pavia, September 1976 (Academia Nazionale Dei Lincei, Roma 1977).

[5] R. W. P. Drever, J. Hough, W. A. Edelstein, J. R. Pugh, and W. Martin, in Proceedings, Pavia 1976.

[6] V. B. Braginsky, Acta Astronautica 2, 535 (1975).

[7] H. D. Wahlquist, J. D. Anderson, F. B. Estabrook and K. S. Thorne, in Proceedings, Pavia 1976.

[8] D. Douglass, in Proceedings, Pavia 1976.

[9] J. Weber, in Proceedings, Pavia 1976.

[10] V. B. Braginsky, in Proceedings, Pavia 1976.

[11] J. Weber, Phys. Rev. Lett. 17, 1228 (1966).

[12] G. W. Gibbons and S. W. Hawking, Phys. Rev. D 4, 2191 (1971).

[13] M. J. Buckingham and E. A. Faulkner, Radio and Elec. Eng. 42, 163 (1972).

[14] D. G. Maeder, Electronics Lett. 8, L113 (1972).

[15] F. Aplin, J. Phys. E., Sci. Instrum. 6, 417 (1973).

[16] P. Kafka, in Comptes Rendus du Colloque International du CNRS sur les Ondes et Radiation Gravitalionelles (CNRS, Paris 1973).

[17] V. B. Braginsky, in Proceedings of the International School of Physics "Enrico Fermi", Course LVI, Varenna, 1972, edited by B. Bertotti (Academic Press, New York and London, 1974).

[18] J. Weber, in Proceedings, Varenna 1972.

[19] E. Amaldi, S. Barbanera, P. Bonifazi, F. Bordoni, M. Cerdonio, C. Cosmelli, U. Giovanardi, I. Modena, G. V. Pallottino, G. Pizzella, F. F. Ricci, G. L. Romani and G. Vannaroni, in Proceedings, Pavia 1976.

[20] R. P. Giffard, Phys. Rev. D 14, 2478 (1976).

[21] H. Hirakawa, K. Narihara and M. K. Fujimoto, Journal of Phys. Soc. of Japan 41, 1093 (1976).

[22] J.P. Richard, Rev. of Sci. Instrum. 47, 423 (1976).

[23] J.-P. Richard, 3rd International Space Relativity Symposium; XXVIIth International Astronautical Congress; Anaheim, California, October 1976. Acta Astronautica 5, 63 (1978)

[24] Wm. S. Davis, Ph.D. Thesis, University of Maryland, 1977 (unpublished)

[25] G. Pizzella, "Optimal Filtering and Sensitivity for Resonant Gravitational Wave Antennas", submitted to Nuovo Cimento.

[26] E. Amaldi, C. Cosmelli, F. Bordoni, P. Bonifazi, U. Giovanardi, G. Vannaroni, G. V. Pallottino and G. Pizzella, Lett Al Nuovo Cimenta 18, 425 (1977).

[27] S. P. Boughn, W. M. Fairbank, R. P. Giffard, J. N. Hollenhorst, M. S. McAshan, H. J. Paik and R. C. Taber, Phys. Rev. Lett. 35, 454 (1977)

[28] R. P. Giffard and J. N. Hollenhorst, Appl. Phys. Lett. 32, 767 (1978).

PREDICTED AND OBSERVED ENERGY AND FLUCTUATION

July 2, 1977	(wideband plus narrowband contributions)		(narrowband contributions)	
	Theory (Eqs. 10 and 12)	from measurement of the slope of the height distribution, figures 6, 7, and 8	Theory (Eqs. 10 and 12)	from measurement of the time average of the data
$x^2 + y^2$ for 1345 to 1811 hours Bar Thermal Temperature 6.6 ± .2 K	9.0 ± .2	7.1 ± 1.1	T_E = 8.6 ± .2	T_E = 6.3 ± 1.1
$x^2 + y^2$ for 2206 to 2344 hours Bar Thermal Temperature 8.1 ± .2 K	10.5 ± .2	12.5 ± 3.4	T_E = 10.1 ± .2	T_E = 11.4 ± 2.3
$(\dot{x}^2 + \dot{y}^2)\tau^2$ for 2206 to 2344 hours Bar Thermal Temperature 8.1 ± .2 K	T_F = 0.59 ± .01	T_F = 0.51 ± .08	0.49 ± .01	.45 ± .07

FIGURE CAPTIONS

1. 134 kg antenna-sensor and filter system.

2. Resonant capacitor sensor providing adjustable coupling to the antenna.

3. Antenna-sensor-preamplifier electrical analog with calibrated reference noise source within dotted lines.

4. Block-diagram of electronics used to record energy and fluctuations.

5. Density distribution of the measurements of the energy of the antenna during a 4 hr. 26 min. experiment with the antenna at 6.6 K.

6. Density distribution of the measurements of the energy of the antenna during a 1 hr. 38 min. experiment with the antenna at 8.1 K.

7. Density distribution of the measured fluctuations of the antenna during a 1 hr. 38 min. experiment with the antenna at 8.1 K.

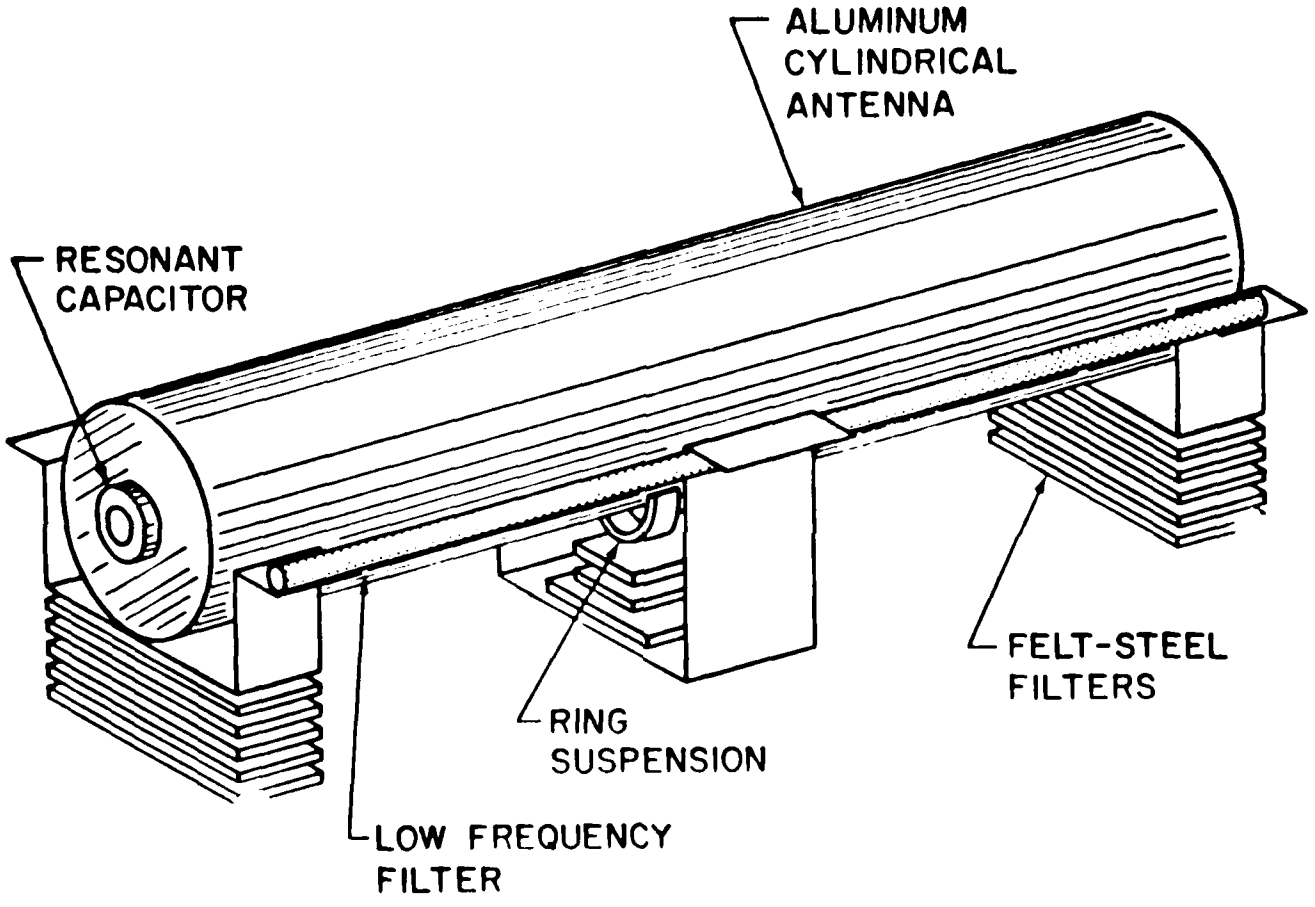
ALUMINUM
CYLINDRICAL
ANTENNA
RESONANT
CAPACITOR
FELT-STEEL
FILTERS
RING
SUSPENSION
LOW FREQUENCY
FILTER

FIGURE 1

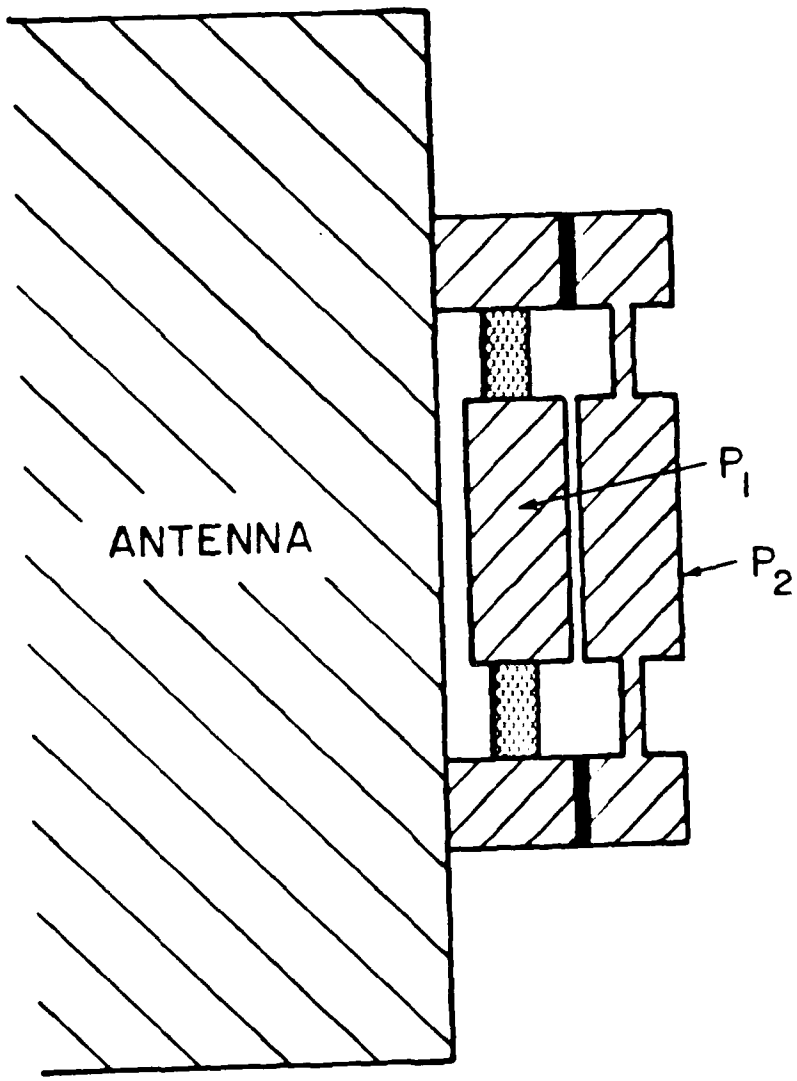

FIGURE 2

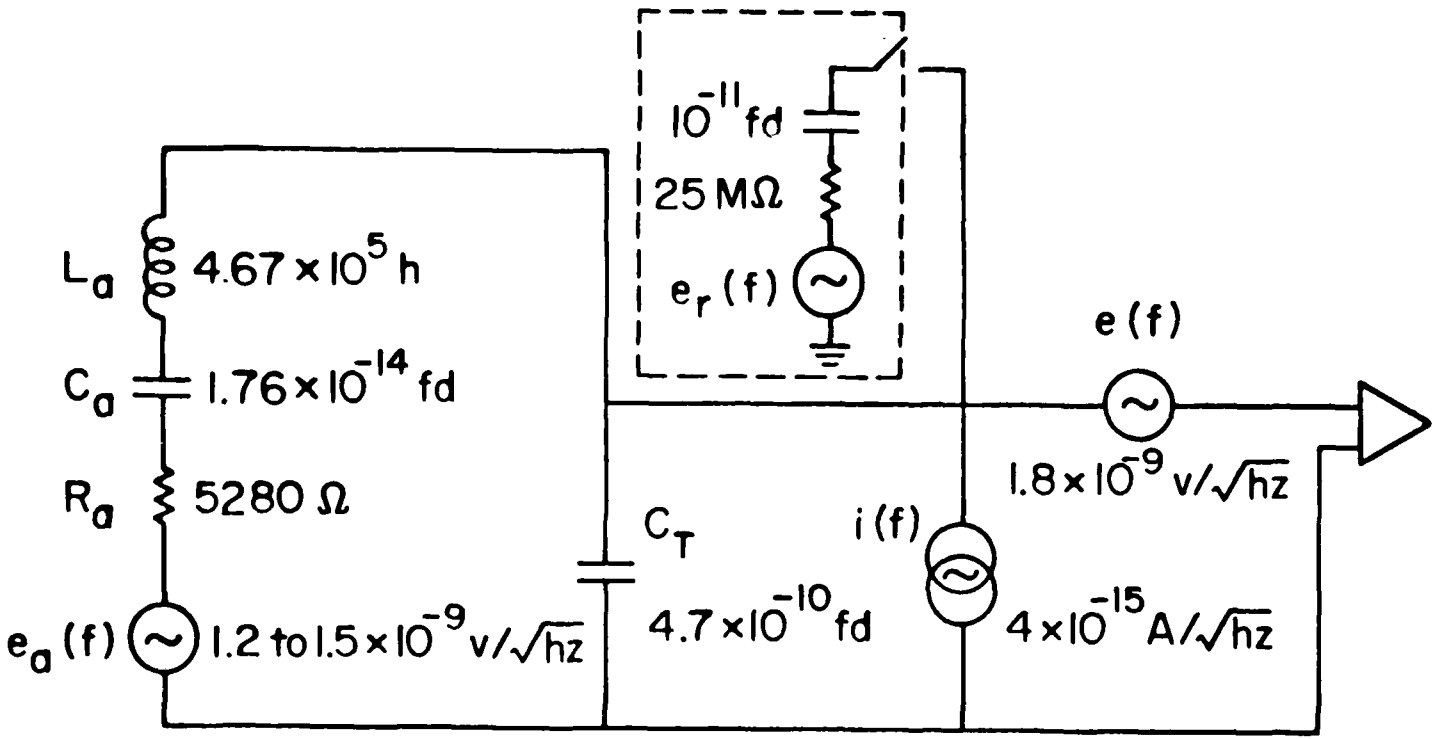
10^{-11} fd
25 MΩ
$e_r(f)$
L_a 4.67×10^{5} h
C_a 1.76×10^{-14} fd
R_a 5280 Ω
$e_a(f)$ 1.2 to 1.5×10^{-9} v/√hz
C_T
4.7×10^{-10} fd
$i(f)$
4×10^{-15} A/√hz
$e(f)$
1.8×10^{-9} v/√hz

FIGURE 3

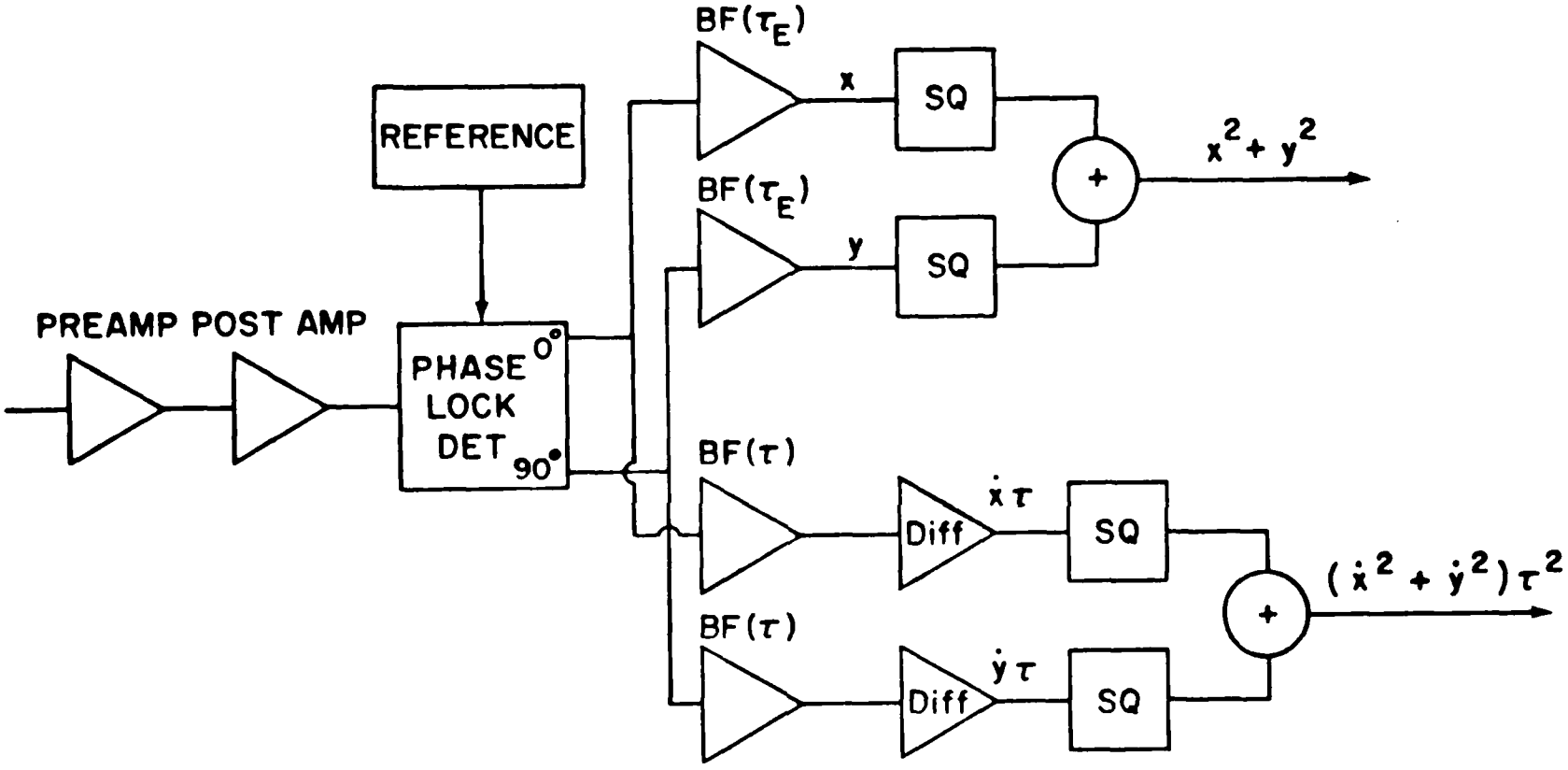

BF(τ), SECOND ORDER BUTTERWORTH FILTER WITH TIME CONSTANT τ

FIGURE 4

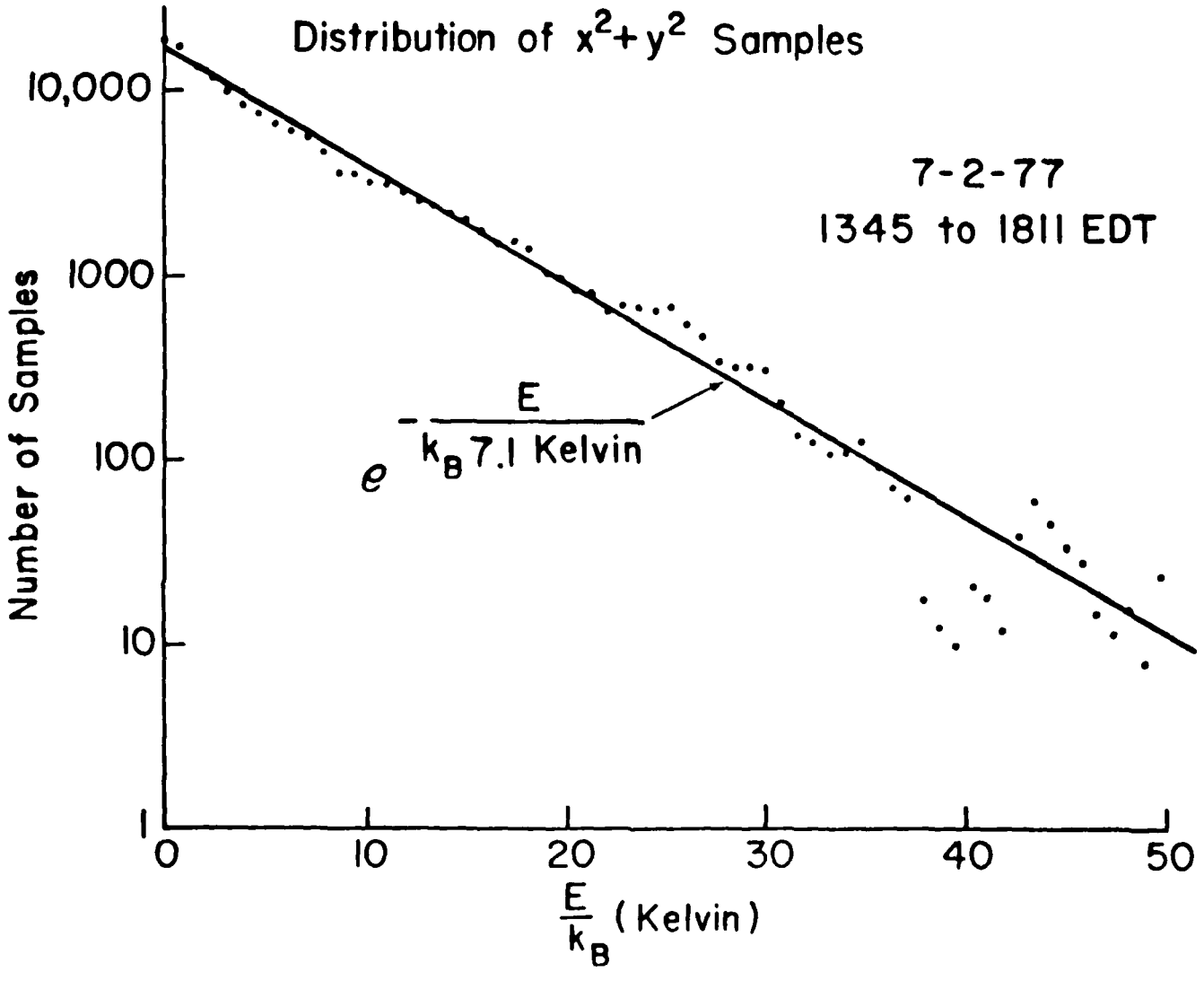
Distribution of x^2+y^2 Samples
7-2-77
1345 to 1811 EDT
Number of Samples
10,000
1000
100
10
1
$e^{-\frac{E}{k_B 7.1 \text{ Kelvin}}}$
0
10
20
30
40
50
$\frac{E}{k_B}$ (Kelvin)

FIGURE 5

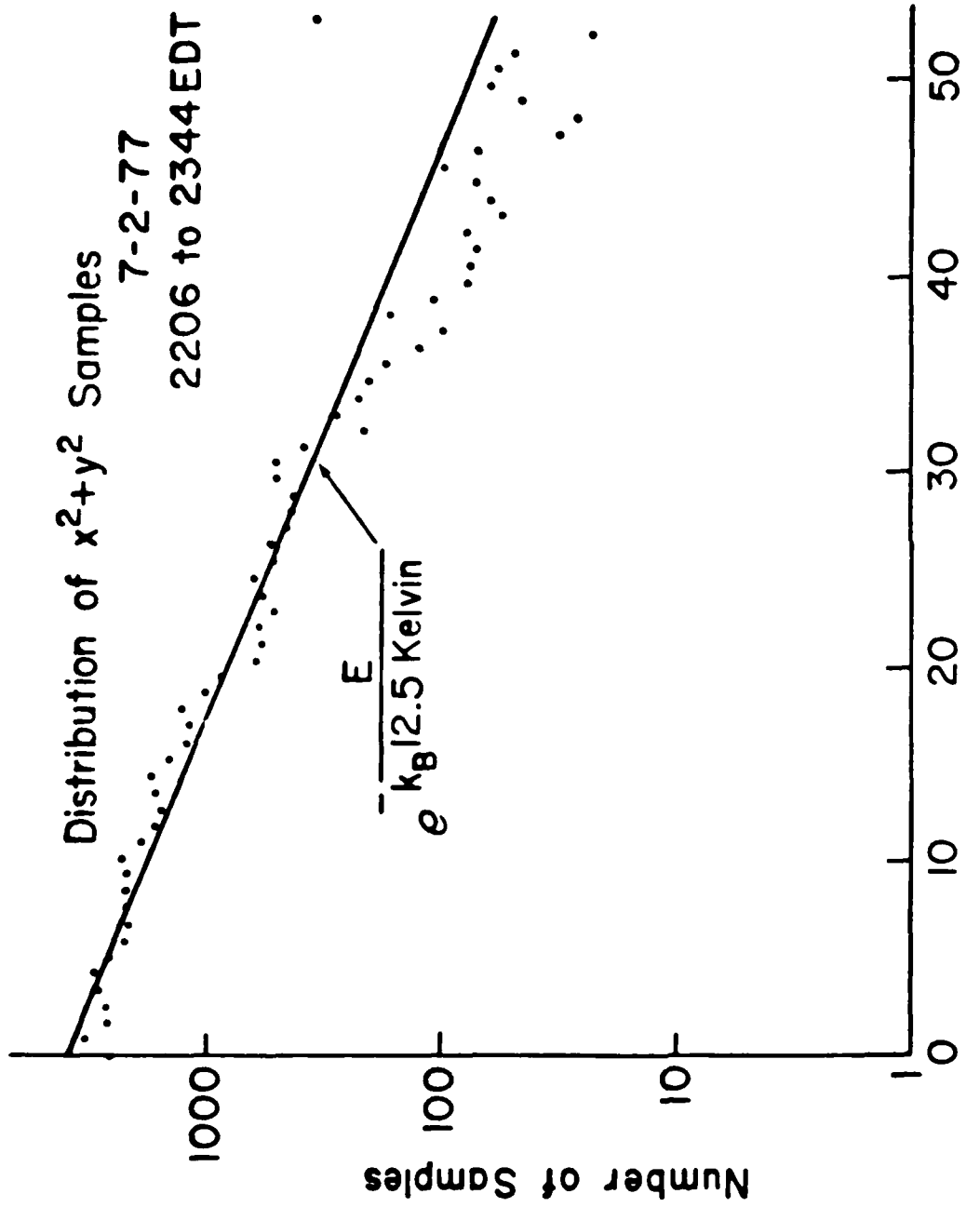
Distribution of x^2+y^2 Samples
7-2-77
2206 to 2344 EDT
$e^{-\frac{E}{k_B 12.5\,\text{Kelvin}}}$
Number of Samples
1000
100
10
1
0
10
20
30
40
50
$\frac{E}{k_B}$ (Kelvin)

FIGURE 6

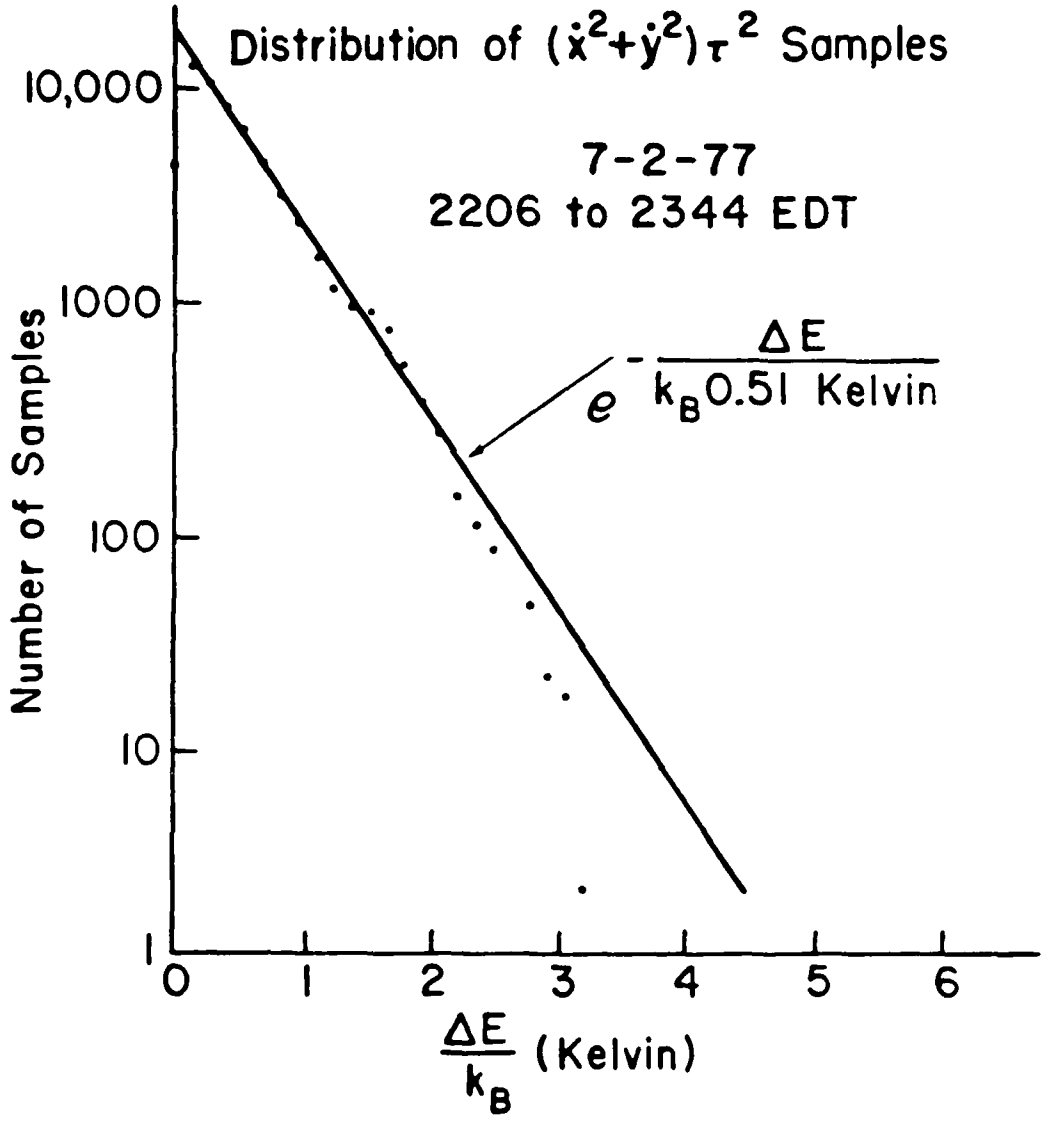
Distribution of $(\dot{x}^2+\dot{y}^2)\tau^2$ Samples
7-2-77
2206 to 2344 EDT
$e^{-\frac{\Delta E}{k_B 0.51 \text{ Kelvin}}}$
Number of Samples
10,000
1000
100
10
1
0
1
2
3
4
5
6
$\frac{\Delta E}{k_B}$ (Kelvin)

FIGURE 7

New Approach to Detection of Small Signals

Most detection systems employ an ensemble of particles in thermal equilibrium. Under these conditions the transition probabilities are proportional to the square of the interaction energy.

A detailed analysis has been carried out for the non equilibrium case, at the very small signal levels where quantum effects are very important. It is found that a wide class of initial quantum states may lead to transition probabilities proportional to the interaction energy, instead of its square. For very small signals this may lead to a large increase in transition probabilities.

The ideas are presented in two following papers "Exchange of Energy With Large Numbers of Particles," and "New Methods for Increase of Interaction of Gravitational Radiation with an Antenna."

EXCHANGE OF ENERGY WITH LARGE NUMBERS OF PARTICLES*

J. Weber

Department of Physics
University of California
Irvine, California 92717

and

Department of Physics and Astronomy
University of Maryland
College Park, Maryland 20742

Abstract

It is proved that to a first approximation it is impossible to exchange significant amounts of energy with an ensemble of particles having wavefunctions with random phases. Possible applications are outlined.

*Supported in part by the National Science Foundation and by the Air Force Office of Scientific Research.

UCI Technical Report #80-13

Introduction

In spectroscopy and in particle detection, energy may be exchanged between incident particles or applied fields, and an ensemble of particles. The wavefunctions of such ensembles may have random phases. It will be shown that the applied fields must introduce some correlations before large amounts of energy can be exchanged.

Energy Exchange With an Ensemble Having Random Phases

Let the ensemble be described by many particle time independent wavefunctions

$$\psi_1, \psi_2, \psi_3, \cdots \psi_n \tag{1}$$

with Hamiltonian

$$H_o \tag{2}$$

and energies

$$E_1, E_2, E_3, \ldots E_n \quad . \tag{3}$$

Possible wavefunctions for the ensemble are

$$\Psi = \sum_j c_j \psi_j e^{\frac{-iE_j t}{\hbar}} \quad , \tag{4}$$

with the coefficients c_j a set of constants.

The ensemble now interacts with incident particles or fields and the Hamiltonian is

$$H_o + H' \quad . \tag{5}$$

A possible wavefunction is again (4), but the c_j must be functions of time. The Schrodinger equation gives

$$\frac{dc_j}{dt} = \frac{1}{i\hbar}\sum_k H'_{jk}c_k e^{\frac{i(E_j-E_k)t}{\hbar}} \qquad (6)$$

with $H'_{jk} = \int \psi_j^* H' \psi_k \, d^3x$.

We require the time derivative of $c_j c_j^*$,

$$\frac{d(c_j c_j^*)}{dt} = c_j \frac{dc_j^*}{dt} + \frac{dc_j}{dt} c_j^* \qquad (7)$$

employing (6) in (7) gives

$$\frac{d}{dt}(c_j c_j^*) = \frac{1}{i\hbar}\sum_k \left(H'_{jk} c_j^* c_k e^{\frac{i(E_j-E_k)t}{\hbar}} - H'^*_{jk} c_j c_k^* e^{\frac{-i(E_j-E_k)t}{\hbar}} \right) . \qquad (8)$$

There are two kinds of terms to consider, in (8). If $j = k$ the two terms on the right side of (8) sum to zero because the Hermitian character of H' guarantees that $H'_{jj} = H'^*_{jj}$. Therefore the remaining terms in (8) are those for which $j \neq k$. The ensemble average of (8) is then

$$\frac{d}{dt}\langle c_j c_j^* \rangle_{ens.} = \frac{1}{i\hbar}\sum_k \left(H'_{jk}\langle c_j^* c_k \rangle_{ens} e^{\frac{i(E_j-E_k)t}{\hbar}} - H'^*_{jk}\langle c_j c_k^* \rangle_{ens} e^{\frac{-i(E_j-E_k)t}{\hbar}} \right) \qquad (9)$$

When the fields are first applied or because of the nature of the interaction, the wavefunctions may have random phases, and it may be true that [1]

$$\langle c_j^* c_k \rangle_{\substack{ens. \\ j\neq k}} = \langle c_j c_k^* \rangle_{\substack{ens, \\ j\neq k}} = 0 \quad . \qquad (10)$$

In any case it is evident that whenever (10) is valid, (9) gives

$$\frac{d}{dt}\langle c_j c_j^* \rangle_{ens} = 0 \quad . \tag{11}$$

The power exchanged is given by

$$\sum_j \frac{d}{dt} \langle c_j c_j E_j \rangle_{ens.} = 0 \tag{12}$$

(12) implies that

$$\Delta \sum_j \langle c_j^* c_j E_j \rangle_{ens} = 0 \tag{13}$$

for a small time Δt, when the phases are random. (13) proves the theorem that:

to a first approximation it is impossible to exchange significant amounts of energy with an ensemble of particles having wavefunctions with random phases.

Applications

In spectroscopy and in some elementary particle detection experiments, an enormous increase in transition rates appears possible by employing equation (9).

Suppose first that we follow the common procedure of allowing radiation to interact with a system in thermal equilibrium. The temperature does not completely specify the system quantum state. Exchange of energy is computed assuming the system to be in some quantum state k. The transition probability W_j to some other state j is given by Fermi's Golden Rule

$$W_j = \frac{2\pi}{\hbar} \left| H'_{kj} \right|^2 \rho(E_j) \tag{14}$$

H'_{kj} is the interaction hamiltonian matrix element and $\rho(E_j)$ is the density of states in the vicinity of the final state. An ensemble average appropriate to the given temperature is then taken.

Instead of following this procedure we may correlate the states by applying local fields so that (9) does not vanish. Exchange of energy will now depend on the quantities

$$\dot{a}_j a_j^* E_j = \frac{1}{i\hbar} \sum_k \int_0^t \left(H'_{jk}\, c_j^* c_k e^{\frac{i(E_j-E_k)t}{\hbar}} - H_{jk}^* c_j c_k^* e^{\frac{-i(E_j-E_k)t}{\hbar}} \right) dt. \quad (15)$$

(15) is now linear in H'_{jk} instead of quadratic as in (14). For experiments in which H' is very small, (15) may lead to an enormous increase in transition rate.

For example in gravitation experiments

$$H' = \sum_{\ell, j} mc^2 R_{o\ell oj} r^{\ell} \xi^j \quad (16)$$

$R_{o\ell oj}$ is the Riemann tensor in normal coordinates. A two mass system with reduced mass m is considered. r^{ℓ} is the vector joining the masses and the gravitational induced relative displacement is ξ^j. For a gravitational collapse in the Virgo cluster the pulse amplitude for $R_{o\ell oj}$ is expected to be smaller than $10^{-33}\,cm^{-2}$.

In weak interaction experiments

$$H' = \frac{g}{\sqrt{2}} \int \langle F | \bar{\psi}_Q \gamma^{\alpha} (1+\gamma_5)\, \psi_{\nu} \bar{\psi}_{\nu} \gamma_{\alpha} (1+\gamma_5) \psi_Q | 0 \rangle\, d^3x \quad (17)$$

In (17) g is the weak interaction coupling constant 1.4×10^{-49} erg cm^3. $\langle F|$ and $|0\rangle$ are the final and original system states respectively. $\bar{\psi}_Q$ and $\bar{\psi}_\nu$ are scatterer and neutrino creation operators, respectively. ψ_Q and ψ_ν are the corresponding annihilation operators. The correlated state transition rates of (9) are linear in the very small quantities $R_{o\ell oj}$ and g. This makes possible a large increase in exchanged energy over the uncorrelated case (14).

Discussion and Conclusion

Energy can be exchanged with matter in thermal equilibrium by means of applied fields. This does not contradict the theorem. Initially the second time derivatives of $c_j c_j^*$ may not vanish. In cases such as magnetic resonance experiments the applied fields eventually modify the wavefunctions, introducing correlations such that $\langle c_j^* c_k \rangle_{\substack{ens \\ j \neq k}}$ and $\langle c_j c_k^* \rangle_{\substack{ens \\ j \neq k}}$ do not vanish.

The rate at which energy can be exchanged with a system is expected to increase if correlations are introduced as suggested by (9), (15), (16), (17).

Footnote

[1] A brilliant discussion of these ensemble averages is given by R. C. Tolman, The Principles of Statistical Mechanics, 1938, sections 78-94, Oxford University Press.

New Method for Increase of Interaction of Gravitational Radiation with an Antenna

J. Weber

Department of Physics and Astronomy
University of Maryland
College Park, Maryland 20742

and

Department of Physics
University of California, Irvine
Irvine, California 92717

University of Maryland Report
#PP 81-002

Abstract

It is shown that there may be a large increase in the interaction of Gravitational Radiation with an antenna prepared in correlated quantum states.

Introduction

The gravitational radiation antenna measures the dynamic space time curvature. Energy absorption is described by a cross section. The fluctuations are computed from statistics appropriate for an ensemble in thermal equilibrium. These antenna fluctuations, together with those originating in the electronics, and the absorption cross section, determine the system sensitivity [1,2].

At low temperatures, polycrystalline 5056 aluminum[3], and single crystals of silicon[4] and sapphire[5], may have quality factors exceeding 5×10^7. The time scale for heat bath interactions then exceeds hours. This suggests the possibility of preparing an antenna in a quantum state very different from the thermal equilibrium state. Such a state might be maintained for a significant fraction of observation times. Here it is shown that an appropriate choice of quantum states may give an enormous increase in the energy absorbed from gravitational radiation.

Theory

Let the antenna consist of two masses, with reduced mass m, and restoring forces. The hamiltonian is given by

$$H = H_A + H_G + H \tag{1}$$

H_A is the hamiltonian of the antenna. For an elastic solid, the antenna hamiltonian may be written as a sum over normal modes. For a "free mass" interferometer antenna, the masses will be supported on mounts, with restoring forces, and a normal mode sum may again be appropriate. H_G is the hamiltonian of the gravitational

radiation field. For the interaction H' we choose

$$H' = mc^2 R_{0\ell 0j} r^{\ell} \xi^{j} \tag{2}$$

Repeated indices ℓ and j are summed over 3 space coordinates. r^{ℓ} is a vector joining the two masses. $R_{0\ell 0j}$ is the Riemann tensor in normal coordinates. The gravitational radiation induced displacement is ξ^{j}. More general kinds of antennas may be described by a sum similar to (2).

Sensitivity of presently planned antennas does require quantum mechanics to describe the antenna. The levels of gravitational flux required to change the occupation number of the antenna mode are large, and the "semiclassical treatment of radiation" is appropriate.

$R_{0\ell 0j}(t)$ is time dependent. Let its Fourier transform be $R_{0\ell 0j}(\omega)$. The wavelength of the largest Fourier components of the radiation is assumed large compared with r^{ℓ}. This is a convenient but not necessary assumption.

Suppose first that the antenna is in thermal equilibrium at temperature T_0. Absorption of energy for this case is calculated assuming the antenna is in an energy eigenstate, then averaging the result over an ensemble with the given temperature. The antenna quantum states are assumed to be those of a harmonic oscillator. The antenna wavefunction is given by

$$\psi = \sum_n a_n(t) u_n(\xi) e^{-\frac{iE_n t}{\hbar}} \tag{3}$$

The time dependent Schroedinger equation may be integrated in successive orders. The initial value of a_k is assumed to be δ_{kn} at time - T/2, at time + T/2, a_k is given by

$$a_k = -\frac{mc^2\left(\frac{2}{\pi}\right)^{1/2}}{\hbar}\int_{-\infty}^{\infty} R_{0k0j}(\omega)\pi^l \xi^j_{kn}\left[\frac{\sin[(\omega_{kn}+\omega)T/2]}{(\omega_{kn}+\omega)}\right]d\omega \,, \tag{4}$$

$\omega_{kn} = (E_k - E_n)/\hbar$

The integration (4) is carried out, then squared to obtain

$$|a_k|^2 = 2\pi\left|mc^2 R_{0k0j}(\omega_{nk})\pi^l \xi^j_{kn}\right|^2/\hbar^2 \tag{5}$$

The absorbed energy U_{Ab} is obtained from (5) making use of the fact that the only non-vanishing harmonic oscillator matrix elements are those for $k = n \pm 1$. Let V^j be a unit vector in the direction of ξ^j_c. Then (5) gives

$$U_{Ab} = (\pi mc^4)\left|R_{0k0j}(\omega_{nk})\pi^l V^j\right|^2 \tag{6}$$

The dependence on the state n has disappeared from (6). The ensemble average is also (6), and (6) agrees with the classical formula.[1]

Let us now explore the possibility of having different initial conditions, with $a_k(0) \neq \delta_{kn}$. The Schroedinger equation then gives

$$\frac{da_k}{d\tau} = \sum_n \left(\frac{mc^2}{i\hbar}\right) R_{0k0j}(\tau)\pi^l \xi^j_{kn} e^{-i\omega_{kn}\tau} a_n \tag{7}$$

We require $\frac{d}{d\tau} a^*_k a_k E_k$, given from (7) as

$$\frac{d}{dt} a_k^* a_k E_k = \sum_n \frac{mc^2 E_k}{\iota\hbar} \left(R_{0l0j}(t) \hbar^l \xi^j_{kn} e^{i\omega_{kn}t} a_k^* a_n \right.$$

$$\left. - R_{0l0j}(t) \hbar^l \xi^j_{kn} e^{-i\omega_{kn}t} a_k a_n^* \right) \tag{8}$$

For the thermal equilibrium case (8) will vanish, since the ensemble averages $\langle a_k^* a_n \rangle$, $\langle a_k a_n^* \rangle$ are zero for $k \neq n$. For $k = n$, the Hermitean character of (2) again leads to zero for (8).

If the quality factor is high, laboratory fields may be employed to correlate the states so that $\langle a_k^* a_n \rangle$, $\langle a_k a_n^* \rangle$ do not vanish for the given antenna. A non-vanishing (8) leads to interaction linear instead of quadratic in the Riemann tensor, as given by (6).

For simplicity let us imagine $a_n = \frac{1}{\sqrt{2}}$, $a_{n+1} = \frac{1}{\sqrt{2}}$ and all other values of a_k zero. Let the Riemann tensor consist of a pulse given by

$$R_{0l0j}(t) = R^M_{0l0j} \sin \omega_0 t \text{ , for } 0 < t < \frac{2\pi}{\omega_0} \tag{9}$$

$R_{0l0j}(t)$ = 0 for all other times.

The absorbed energy U^c_{Ab} is the change in the quantity $|a_n|^2 E_n + |a_{n+1}|^2 E_{n+1}$, given by

$$U^c_{Ab} = \left(m\hbar\omega_{n+1,n} \left[(n+1)/2 \right] \right)^{1/2} c^2 R^M_{0l0j} \hbar^l V^j \left(\frac{\omega_0}{\omega^2_{n+1,n} - \omega_0^2} \right) \sin \left(\frac{2\pi \omega_{n+1,n}}{\omega_0} \right) \tag{10}$$

For expected small values of the Riemann tensor, (10) may be enormously greater than the thermal equilibrium value (6).

Conclusion

The use of correlated states, as implied by (10), leads to a possible large increase in the interaction of gravitational waves with an antenna. As long as there are no other interactions, the energy fluctuations of such a prepared system are zero. It is by no means obvious that an antenna can be prepared in such states, and that the unwanted interactions can be kept sufficiently small to result in major improvements in signal to noise ratio. The possibilities of such improvement are now being studied.

Classical physics leads to energy exchange linear in the Riemann tensor if the initial antenna amplitude is large, and the Riemann tensor has an appropriate time dependence. Quantum mechanics gives, for correlated states, energy exchange linear in the Riemann tensor for all initial amplitudes, and without restrictions on the time dependence of the Riemann tensor.

This research was supported in part by the National Science Foundation and in part by the Air Force Office of Scientific Research.

References

1. J. Weber, Einstein Centenary Volume of the International Society on General Relativity and Gravitation.
2. K. Thorne, Rev. Mod. Physics, April 1980.
3. Suzuki, Tsubono, Hirakawa, Physics Letters 67A, 1, 2, 1978.
4. J. Weber, D. H. Douglass, Jr., Gravitazione Sperimentale Pavia, September 17-20, 1976, p. 214, 273.
5. Bagdasarov, Braginsky, Mitrofanov, Krystallographia 19, 883, 1974.

Experiment to Search for Correlated State Effects

The most simple system is a spin $\frac{1}{2}$ ensemble since each particle has only two possible states. In order to search for effects of correlations a proton nuclear magnetic resonance experiment was set up, in the following way.

A low power oscillator source and radio frequency bridge was first employed, and the proton lines observed. Then a second oscillator of much higher power, displaced in frequency from the low power oscillator, was introduced. As the magnetic field was swept the high power oscillator first produced correlations. These modified the observed line intensity for the second oscillator. Changes of intensity roughly 20 percent were observed, and ascribed to correlations.

These results are tentative. The experiments will be repeated in order to obtain more quantitative checks.

DESIGN OF THE MILLI-KELVIN CRYOSTAT

Low temperature physics is a frontier which is explored by going to successively lower temperatures. The study of the properties of single crystal silicon and sapphire by our group at the University of Maryland has indicated that temperatures below that of liquid helium are needed in order to more thoroughly understand the mechanisms of acoustic loss in these crystals. Toward this we have recently acquired a He^3 - He^4 dilution refrigerator from the S.H.E. Corporation. This device will allow us to reach temperatures of approximately .02 K. Because of the size of the crystals under study, however, a fairly large volume would have to be cooled. This necessitated the construction of a liquid helium cryostat of a size and configuration unavailable commercially. This section describes the design of this cryostat. Also the design of the experiment vacuum chamber and adaptor for the dilution refrigerator insert is described.

STRUCTURE

A drawing of the cryostat appears in Figure 1. The dimensions shown allow a final .02 K volume of $\sim$35 ℓ.

The outer wall of the cryostat is at room temperature and is 25" diameter X 72" long. Inside this is the liquid nitrogen shield which is a shell formed by two co-axial cylinders of 22" and 19" diameters X 68" long. This liquid nitrogen tank has a volume of 108 ℓ. Across the bottom of this tank is a 1/16" thick copper plate for thermal shielding. Also for thermal shielding is a 1/16" thick copper liner welded to the inside of the tank and extending 48" from the top. The entire liquid nitrogen tank is suspended from three stainless steel pipes 1/4" I.D. X 3/32" wall thickness.

Thermal considerations lead to the use of a fiberglass vessel for the inner container where the liquid helium would be. It is 16" I.D. X 70" long X 1/4" wall thickness. The vessel mates at room temperature to the rest of the cryostat with a teflon gasket. The fiberglass is made from Hetron 31, a polyester resin made by Ashland Chemicals. Typical properties of a Hetron 31 laminate are shown in Table 1.

To the bottom of the liquid nitrogen tank was thermally attached a container holding ~3 lbs of Type 5A Linde molecular sieve material. This was to absorb any residual nitrogen left in the vacuum space after pumping. A graph of the absorbance of Type 5A is shown in Figure 2. Figure 3 shows the modified dilution refrigerator insert. The available experimental space inside the .8 K thermal shield is an upright cylinder 16" tall X 13' diameter. This represents a volume of 35 ℓ.

THERMAL CALCULATIONS

Heat Leak into the Liquid Helium

Conduction paths into the liquid helium are through the walls of the fiberglass vessel and through the support structure of the experimental insert. The thermal conductivity of the fiberglass was known only at room temperature ($2.175 \times 10^{-3} \frac{W}{cm\ K}$). However, since the glass fibers contribute much to the properties of fiberglass, it was decided to use the thermal conductivity curve for fused quartz normalized at room temperature to the value for fiberglass. Using the data, from the American Institute of Physics Handbook, the following results were obtained for fiberglass:

$$K_{F1} \equiv \int_{4.2}^{77} \lambda(T)\, dT \approx .0781 \quad \frac{w}{cm}$$

and

$$K_{F2} \equiv \int_{77}^{300} \lambda(T)\, dT \approx .341 \quad \frac{w}{cm}$$

If the thermal gradient is from room temperature at the top of the cryostat to 4.2 K at the top of the liquid helium and we assume the level of helium is 24" from the top (this is the highest level), we get the heat leak from this source to be $\dot{Q}_{c1} = .56\,w$.

It is instructive at this point to compare the fiberglass vessel to a similar vessel made of stainless steel. If stainless steel were used for the innermost shell, the minimum thickness would be 0.04". This leads to a heat leak of:

$$\dot{Q}_{S.S.} = \frac{A}{\ell} \int_{4.2}^{300} \lambda(T)\, dt = (.21\,cm)\left(30.4\ \frac{w}{cm}\right) = 6.5\,w$$

Clearly, even though the fiberglass needs to be much thicker to withstand the pressure, it is still much better thermally than stainless steel.

To reduce the above heat leak even further, the fiberglass was heat sunk to the liquid nitrogen 6" from the top of the fiberglass vessel. Copper braid was wrapped around the circumference of the vessel and covered with Hetron 31 resin. This band was then connected to the liquid nitrogen tank via six copper braids equidistant around the circumference. Each copper braid was ~12" long X .48 cm^2 cross-section. The thermal conductivity of copper at 77 K is approximately 6 $\frac{w}{cm\,K}$. If we assume that the temperature T where the braid attaches to the fiberglass is near 77 K, we can

equate the power through the braid to the power through the fiberglass to find T.

$$(6\ \frac{w}{cm\ K})\ (T - 77)\ (.095\,cm) = (.341\ \frac{w}{cm})\ (5.32\,cm)\ (\frac{300 - T}{300 - 77}) \rightarrow T \approx 80\,K$$

where the left side of the equation is the conductivity through the copper and the right side that through the fiberglass. With the fiberglass vessel heat sunk at 80 K we find the new $\dot{Q}_{c1}$ = .14 w. The support for the experimental insert vacuum chamber is mainly the stainless steel pipes used for gas circulation as part of the dilution refrigerator operation. Since the dilution refrigerator was designed for a much smaller vacuum chamber than the one we will use, four 1/4" G-10 fiberglass rods were added to take up some of the weight. The heat leak for these is:

$$\dot{Q}_{c2} = (.419\ \frac{w}{cm})\ (.021\,cm) = .009\,w$$

The total heat leak due to conductivity is $\dot{Q}_c$ = .15 w. (The heat leak due to the pipes will be considered later.)

Around the sides and bottom of the vessel were wrapped 10 layers of aluminized mylar to reduce thermal radiation. The heat leak from this is $\dot{Q}_{R1}$ = 8.9 m w. The inside of the vessel was plugged with styrofoam insulation to reduce convection and to channel the boil-off gas to the walls of the container. This plug consisted of 9 layers of styrofoam each ~2.5" thick sandwiched with aluminized mylar. The heat leak due to radiation from this direction would be $\dot{Q}_{R2}$ = .12 w. The total heat leak into the liquid helium is $\dot{Q}_T$ = .28 w.

If we assume the boil-off gas leaves the cryostat with a temperature of ~20 K the heat capacity of the helium would be ~12 KJ/liquid liter. This leads to a boil-off rate of ~2 ℓ/day. Data from the S.H.E. Corporation indicates that the contribution to boil-off rate from the stainless steel pipes of the insert and from consumption of liquid helium in a helium

cold-plate would be about 5 ℓ/day. The total boil-off rate is, therefore, 7 ℓ/day. Since the liquid helium volume is about 50 ℓ, this rate should allow a 7 day running time for the dilution refrigerator.

Heat Leak into the Liquid Nitrogen

The heat leak into the liquid nitrogen due to conduction would be through two paths. The first conduction path is the supporting stainless steel pipes. The area of these pipes is .653 cm^2 each. The thermal conductivity for stainless steel is, $\int_{77}^{300} \lambda(T)\, dT = 27.2 \frac{w}{cm}$. If we let the the thermal gradient go from 300 K to 77 K over a distance of 1", we get $\dot{Q}_{c1}$ = 21.0 w. The other conduction path is the copper braid. The total area for these braids is 2.9 cm^2. If we let $K_{cm} = 6 \frac{w}{cm\ K}$ and ΔT = 3 K, we get $\dot{Q}_{c2}$ = 1.7 w. The total heat leak due to conduction into the nitrogen is $\dot{Q}_c$ = 22.7 w.

The liquid nitrogen tank is also insulated with 10 layers of aluminized mylar. The radiation heat leak from room temperature is Q_R = 2.9 w. The total heat leak into the liquid nitrogen is, therefore,

$$\dot{Q}_T = 25.6\,w.$$

If we assume the boil-off gas leaves the cryostat at 100 K, we get a boil-off rate of 11 ℓ/day. Since the copper thermal shield extends only to 48" from the top, we will assume the tank is empty when the level reaches that point. This represents a volume of 76 ℓ and also gives a running time of about 7 days.

These calculations indicate that, with this cryostat, an experiment may be run for about a week without the noisy interruption of adding cryoliquids.

MAGNETIC LEVITATION

In order to isolate the crystals under investigation as much as possible they will be magnetically levitated. This is accomplished by coating the bars with a thin layer of niobium. When the niobium goes superconducting it excludes any magnetic fields from the interior of the bar. This creates a magnetic pressure given approximately by $p = \frac{B^2}{2\mu_0}$ (all units in MKS). This pressure is exerted against the bar and, if the field is properly shaped, will "float" the bar. (The proper way to calculate the necessary field strength is to recognize that the magnetic field must vanish at the superconducting boundary and solve the resulting image problem; however, the above equation serves as a first approximation.) If we consider a silicon bar, 7 inches by 2 inches diameter, the necessary magnetic field strength to levitate is ~500 gauss. The first critical field of niobium is 1980 gauss at T = 0 and ~1600 gauss at T = 4.2 K. Since the applied field is below the first critical field, the London equation can be used to calculate the penetration depth of the magnetic field and therefore the thickness of the niobium coating needed. The London equation states that the magnetic field varies exponentially with distance into the superconductor with characteristic length λ_L called the London penetration depth. This penetration depth must be modified when $\ell \ll \xi_0$. Where ℓ is the mean free path length of the normal electrons and ξ_0 is the coherence length of the superconducting electrons. The penetration depth becomes $\lambda \approx \lambda_L (\frac{\xi_0}{\ell})^{1/2}$. Since at low temperatures electron scattering is dominated by lattice imperfections and impurities, the worse case for niobium would be ℓ = 3.3 Å which is the lattice spacing. With λ_L = 390 Å and ξ_0 = 380 Å this gives λ = .4 μm. Therefore, a coating ~1 μm thick would be adequate.

The coating process will be a chemical vapor deposition. In this process a low melting point niobium compound is evaporated and allowed to come in contact with the crystal. The crystal has been heated so that the niobium compound dissociates on contact and pure niobium is deposited. This method was chosen over the more energetic sputtering or plasma spray techniques of deposition so as to minimize damage to the crystal. The resulting coating will be 5 - 20 μm thick.

When a flux coil is near a superconducting surface, its inductance is a function of distance from the surface. To stabilize the bar in the direction parallel to the cylinder axis, two flat coils will be positioned at the ends of the bar. By measuring the ac component of the inductance of the coils we can instrument the bar. Since nothing will be touching the crystals except a thin layer of niobium, we expect to get good isolation.

COMPLETION OF THE GAS HANDLING SYSTEM

The dilution refrigerator purchased from the S.H.E. Corporation includes a Gas Handling System (GHS) which controls the flow of He^3 and He^4 into the dilution refrigerator. An option offered by SHE is to buy only that part of the GHS which handles the more expensive He^3. In order to purchase a more powerful refrigerator we took the half system. The second half of the GHS is used for pumping and purging with He^4 and N_2. We have just completed construction of this portion so as to have all the capabilities of the complete GHS. This completed GHS gives us one of the most powerful dilution refrigerators commercially available and should allow use to reach temperatures <20 mK.

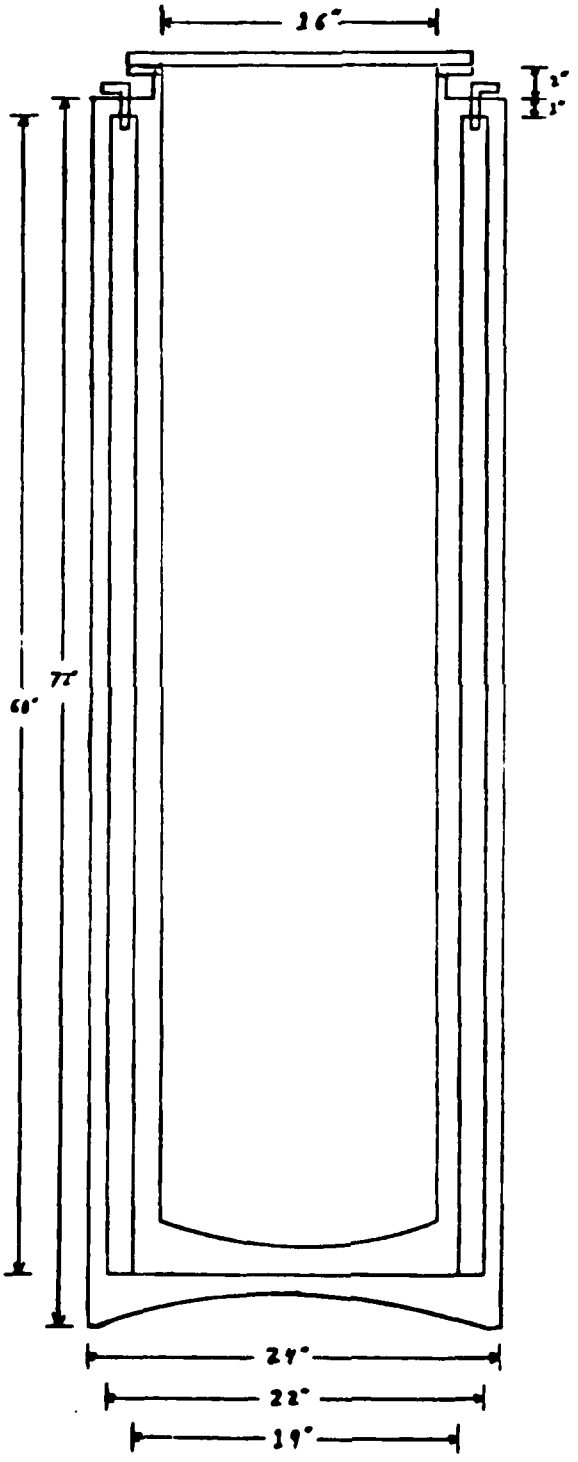

Figure 1. Milli-Kelvin cryostat

ISOTHERM DATA SHEET NO. 62
ADSORBATE: Nitrogen
TEMPERATURE: −196°C to −75°C

TITLE: Nitrogen Adsorption
ADSORBENT: Molecular Sieve Type 5A Pellets

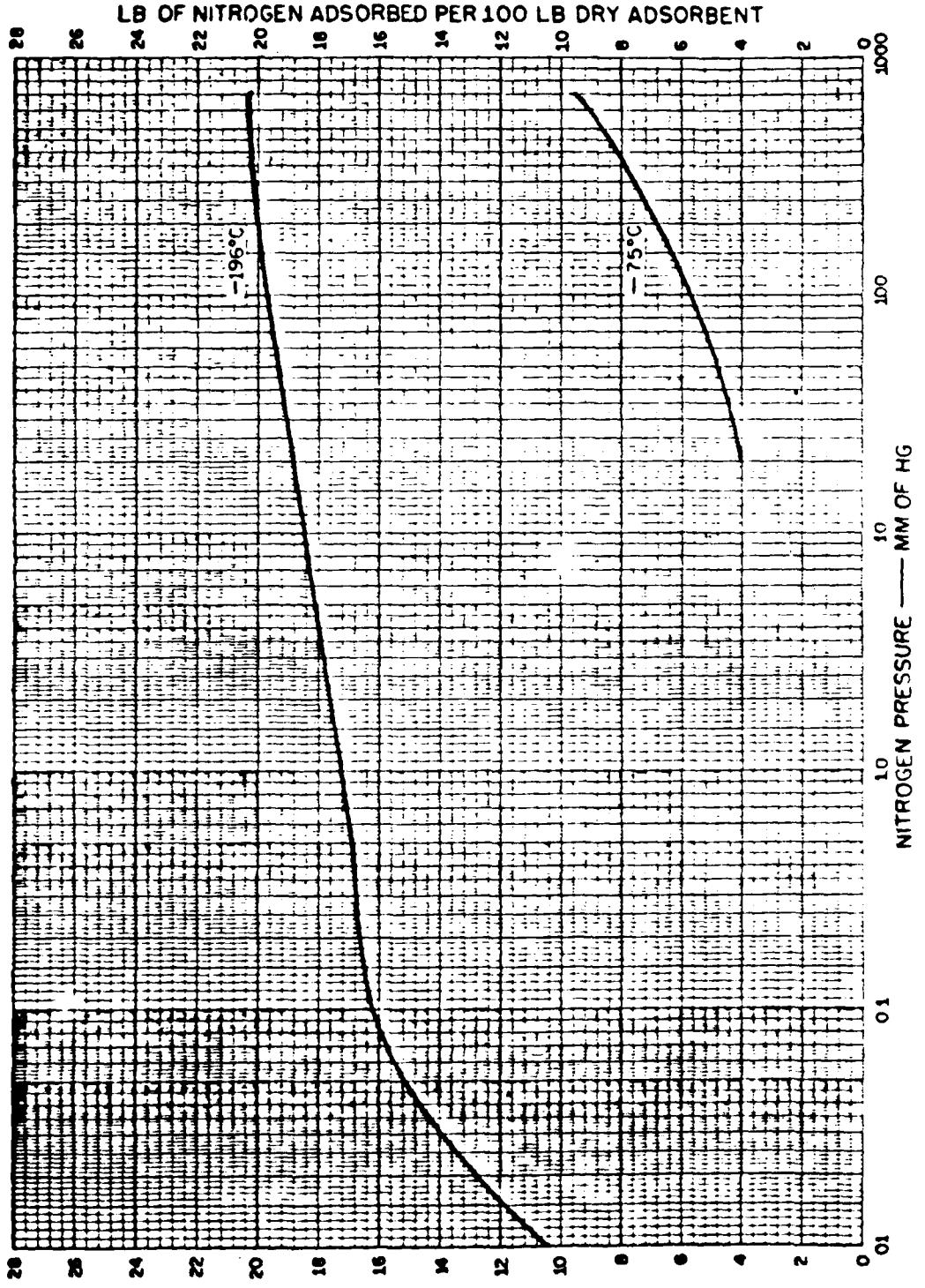

Figure 2. Linde type 5A molecular sieve adsorbance

UNION CARBIDE ADSORBENTS & CATALYSTS

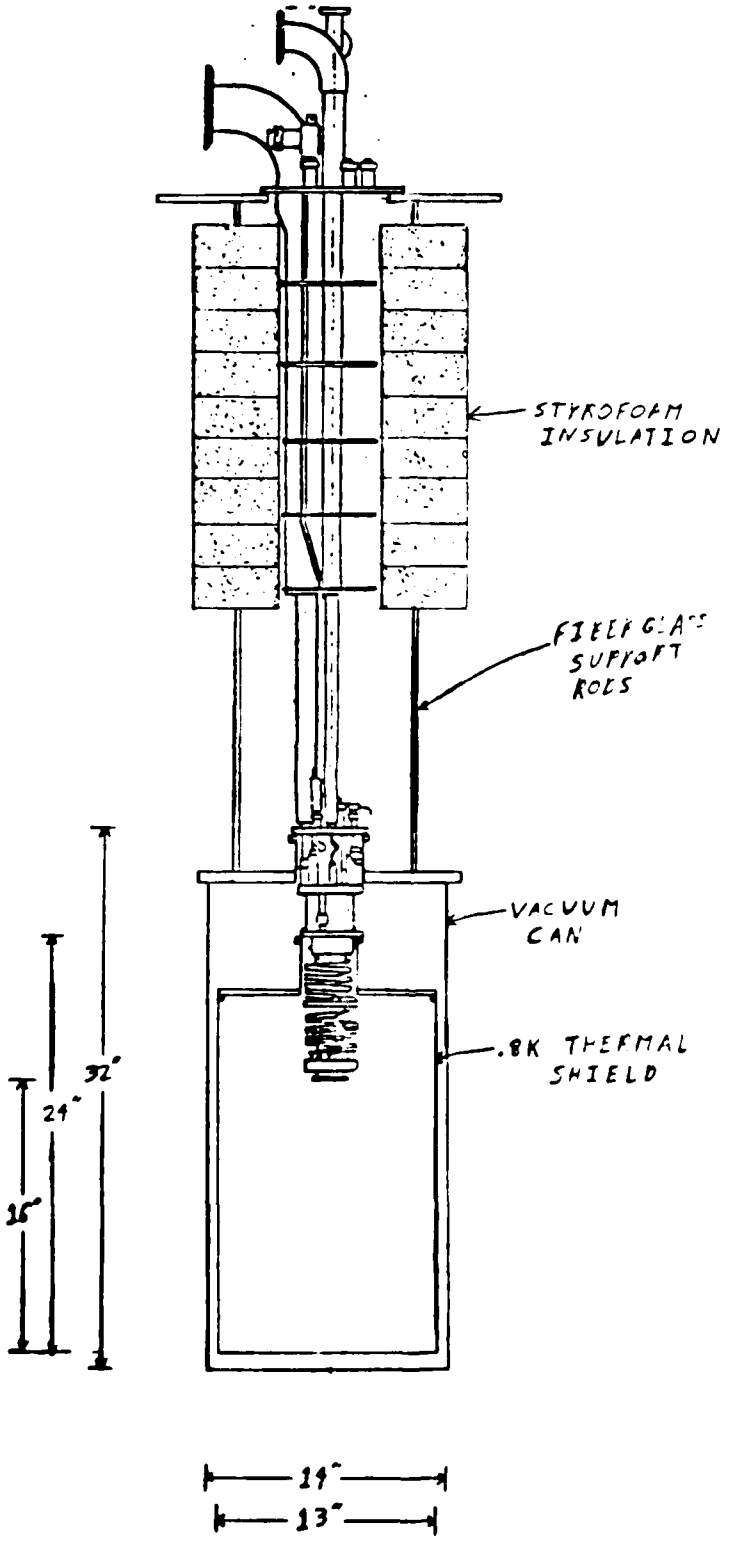

Figure 3. Dilution refrigerator insert and vacuum can

HETRON 31 LAMINATES

60% Glass Cloth, 181 Volan A, Press Cured, 1/8 inch

TENSILE PROPERTIES (Average of 5)

	R.T.	-110°F	-320°F	-424°F
Ultimate Strength x 10^3 psi	50.0	68.1	105.3	100.0
Initial Modulus x 10^6 psi	2.97	3.24	3.87	3.92

FLEXURAL PROPERTIES (Average of 5)

Ultimate Strength x 10^3 psi	71.2	104.1	126.7	129.0
Initial Modulus x 10^6 psi	3.24	3.47	4.18	4.26

EDGEWISE COMPRESSION PROPERTIES (Average of 5)

Ultimate Strength x 10^3 psi	19.9	41.2	68.5	67.3
Modulus x 10^6 psi	1.64	1.85	2.36	2.71

Table 1. Hetron 31 fiberglass properties

APPENDIX

THE MEASUREMENT OF NOISE IN MONOCRYSTALS AT CRYOGENIC TEMPERATURES: EXPECTED PROBLEMS AND PROPOSED SOLUTIONS

Wm. S. Davis

April 19, 1979

Introduction

It is planned to make noise measurements of monocrystals of sapphire and/or silicon near the thermodynamic temperature of 5 Kelvin. This report describes some of the expected problems of making such noise measurements with high elastic Q materials and low coupling. Solutions to the problems are also discussed.

Table I summarizes the properties of the silicon and sapphire crystals. Each crystal is supported by a fourpoint rigid suspension built by Jean-Paul Richard. These are shown in figures* 1 and 2. Each is coupled to a small piezoelectric ceramic transducer (pzt-4). For the silicon the transducer is epoxied to the mount as shown in figure 1. The transducer for the sapphire is epoxied directly onto the crystal itself.

Figure 3 shows the well known equivalent circuit for one mode of an elastic solid coupled to a transducer and amplifier. Resistors R_1 and R_2 couple Brownian motion energy into the crystal mode. This energy is proportional to the thermal temperature T. Other processes such as non-equilibrium effects and the current noise of the amplifier also put energy into the crystal. The effective noise temperature is defined for the purposes of this report to be the thermal temperature which R_1 and R_2 would have to have to produce the same noise energy in the crystal that all the sources combined produce. It is the goal of the experiment to measure the effective noise temperature for the fundamental mode of the silicon and/or sapphire crystals near 5 Kelvin.

The problems in making the noise measurement include the following. High Q crystals "ring" for a long time. The noise measurement can be disrupted if the amplitude of the ringing greatly exceeds the noise level. The present

* Each section of this report has figures numbered independently.

AD-A090 805 MARYLAND UNIV COLLEGE PARK DEPT OF PHYSICS AND ASTRONOMY F/G 20/1
INVESTIGATION OF NOISE IN SOLIDS AT LOW TEMPERATURES.(U)
AUG 80 W S DAVIS, K KRACK, J RICHARD, J WEBER F49620-77-C-0065
UNCLASSIFIED AFOSR-TR-80-1008 NL

2 OF 2
AD A090805

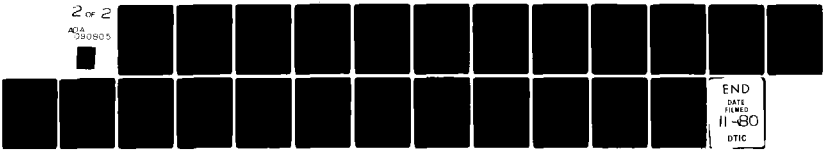

END
DATE FILMED
11-80
DTIC

crystal, transducer, and amplifier combination requires a very small bandwidth to see the energy noise of the crystal over the wideband noise of the amplifier. This in turn requires a very stable reference frequency tuned accurately to the crystal resonance. A relatively small bandwidth is also required in one of the intermediate stages of amplification. Before making the noise measurements electronics must be carefully designed, built, and tuned to solve the above foreseeable problems. This is discussed in the following sections.

Summary of Noise Analysis

Consider the electronics of figure 4. x(t) and y(t) are output voltages which are slowly varying functions of time. Let G be the overall gain of the electronics, and let B(ω) be the complex transfer function of the Butterworth low pass filter after its contribution to the overall gain has been factored out.

$$B(\omega) = \frac{1}{1 + i\omega\sqrt{2}\,\tau_f - \omega^2\tau_f^2}$$

$$|B(\omega)|^2 = \frac{1}{1 + \omega^4\tau_f^4}$$

$$B(0) = 1$$

If the input voltage to the preamp is noise only, described by spectral density $e_{in}(\omega)$, then

$$\langle x^2 + y^2 \rangle = G^2 \int_{-\infty}^{+\infty} \frac{1}{2}\left[\left|B(\omega-\omega_r)\right|^2 + \left|B(\omega+\omega_r)\right|^2\right] e_{in}^2(\omega)\, d\omega$$

$$= G^2 \int_{-\infty}^{+\infty} \frac{e_{in}^2(\omega+\omega_r)\, d\omega}{1 + \omega^4\tau_f^4} \qquad (1)$$

where ω_r is the reference frequency of the lock-in amplifier. Further linear filtering of x and y, either analog or digital, will modify the above noise equation. For filtering relevant to this report,

$$\langle \dot{x}^2 + \dot{y}^2 \rangle \tau_f^2 = G^2 \int_{-\infty}^{+\infty} \frac{\omega^2 \tau_f^2}{1 + \omega^4 \tau_f^4} e_{in}^2 (\omega + \omega_r) \, d\omega \quad (2)$$

$$\langle (x + \dot{x}\tau_c)^2 + (y + \dot{y}\tau_c)^2 \rangle =$$

$$G^2 \int_{-\infty}^{+\infty} \frac{1 + \omega^2 \tau_c^2}{1 + \omega^4 \tau_f^4} e_{in}^2 (\omega + \omega_r) \, d\omega \quad (3)$$

It can be shown that in the vicinity of the resonance of the crystal (figure 3) the voltage spectral density at the preamp input is given by,

$$e_{in}^2 (\omega + \omega_o) = e_f^2 (\omega_o) + e_2^2 (\omega_o) + \frac{J_f^2 (\omega_o)}{\omega_o^2 C_2^2}$$

$$+ \frac{(\beta Q)^2}{1 + \omega^2 \tau_o^2} \left[e_1^2 (\omega_o) + e_2^2 (\omega_o) + \frac{J_f^2 (\omega_o)}{\omega_o^2 C_2^2} \right] \quad (4)$$

The above assumes the following:

$$|\omega| << \omega_c$$

$$\beta Q \frac{1}{\omega_0 C_2 R_2} >> 1$$

$$Q^2 \beta >> 1$$

and that the spectral densities of the noise sources are slowly varying with frequency. Notice that the input spectral density divides naturally into two parts, a wideband part (the first three terms) and a narrowband part (term with $1 + \omega^2 \tau_c^2$ in denominator). The narrowband term is proportional to the spectral density of the energy of the crystal for the mode being observed. The noise energy of the crystal comes from $e_1(\omega)$, $e_2(\omega)$, $j_f(\omega)$, and possibly other sources which are not included in the analysis. If thermal Brownian motion is the only source of noise then

$$e_1^2(\omega_0) + e_2^2(\omega_0) = \frac{2}{\pi} k T (R_1 + R_2)$$

The effective noise temperature (T_n) of the $R_1 + R_2$ combination is defined for this report to be the thermodynamic temperature they would have to have to produce the same narrowband noise as all the noise sources combined. Thus,

$$T_n = \frac{e_1^2(\omega_0) + e_2^2(\omega_0) + \frac{j_f^2(\omega_c)}{\omega_0^2 C_3^2} + \begin{matrix}\text{other} \\ \text{sources}\end{matrix}}{\frac{2}{\pi} k (R_1 + R_2)}$$

It should be emphasized that this noise temperature describes only the narrowband part of the noise, those processes contributing to noise energy in the crystal mode itself.

Let $e_w^2(\omega_o)$ be the sum of the three wideband terms,

$$e_w^2(\omega_o) = e_f^2(\omega_o) + e_2^2(\omega_c) + \frac{j_f^2(\omega_c)}{\omega_c^2 C_2^2}$$

Then equation 4 for the input spectral density can be rewritten,

$$e_{in}^2(\omega+\omega_o) = e_w^2(\omega_c) + \frac{1}{1+\omega^2\tau_o^2}\,\frac{2\beta Q k T_n}{\pi \omega_c C_2}$$

The results for calculations of the linear filtering given by equations 1, 2, and 3 are shown next. It is assumed that the reference frequency is equal to the crystal frequency, $\omega_r = \omega_c$.

$$\langle x^2 + y^2 \rangle =$$

$$G^2 e_w^2(\omega_c)\frac{\pi}{\sqrt{2}\,\tau_f} + \frac{G^2 2\beta Q k T_n}{\omega_c C_2 \sqrt{2}\,\tau_f}\,\frac{\frac{\tau_f}{\tau_c} + \sqrt{2}}{\frac{\tau_o}{\tau_f} + \frac{\tau_f}{\tau_c} + \sqrt{2}} \qquad (5)$$

$$\langle \dot{x}^2 + \dot{y}^2 \rangle \tau_f^2 =$$

$$G^2 e_w^2(\omega_o)\frac{\pi}{\sqrt{2}\,\tau_f} + \frac{G^2 2\beta Q k T_n}{\omega_o C_2 \sqrt{2}\,\tau_f}\,\frac{\frac{\tau_f}{\tau_o}}{\frac{\tau_c}{\tau_f} + \frac{\tau_f}{\tau_o} + \sqrt{2}} \qquad (6)$$

$$\langle (x + \dot{x}\tau_o)^2 + (y + \dot{y}\tau_o)^2 \rangle =$$

$$G^2 e_w^2(\omega_o)\frac{\pi}{\sqrt{2}\,\tau_f}\left(1 + \frac{\tau_o^2}{\tau_f^2}\right) + \frac{G^2 2\beta Q k T_n}{\omega_o C_2 \sqrt{2}\,\tau_f} \qquad (7)$$

No approximations were made in evaluating the integrals for the above. Note the following relationship,

$$\langle (x + \dot{x}\tau_o)^2 + (y + \dot{y}\tau_o)^2 \rangle =$$

$$\langle x^2 + y^2 \rangle + \langle \dot{x} + \dot{y}^2 \rangle \tau_o^2$$

Table I gives the expected values for the elements of the equivalent circuits of the silicon and sapphire. There is an expected error of ≤ 20% for the sapphire parameters. Due to the uncertainity of β for silicon only limits exist for several of its parameters. The voltage and current noise of the FET amplifier to be used has not yet been measured at 3465 and 18642 hertz. At 1755 hz the noise was measured as,

$$e_f(\omega) = \frac{1.8 \times 10^{-9} \frac{volts}{\sqrt{hertz}}}{\sqrt{2\pi}} = .72 \times 10^{-12} \frac{volts}{\sqrt{rad/sec}}$$

$$j_f(\omega) = \frac{4.0 \times 10^{-15} \frac{amps}{\sqrt{hertz}}}{\sqrt{2\pi}} = 1.6 \times 10^{-15} \frac{volts}{\sqrt{rad/sec}}$$

for BF817 FET

For the parameters in the table the effect of the current noise can be neglected. The expected noise temperature for both crystals is the thermal temperature of 4 to 5 Kelvin. R_2 has not been directly measured yet for either crystal. If the electronic Q of the piezoelectric transducers is estimated conservatively at 50 then the effect of R_2 on the Q of the crystal, the narrowband noise, and the wideband noise can be neglected.* Next the time constant τ_f of the filters

*Mechanical losses in the piezoelectric, the epoxy, and the suspension contribute to R_1.

will be chosen so that the expected wideband and narrowband outputs are equal. Table II lists the values for τ_f and the expected total noise. These numbers are to be used at present for design purposes only. After better measurements of the noise and parameters are made there could be considerable differences.

To obtain the narrowband part of the noise, first the total noise (wideband plus narrowband) will be measured. The wideband part alone can be determined by slightly detuning the reference oscillator of the lock-in amplifier so that the narrowband part falls outside the overall bandwidth. Substracting then yields the average narrowband output. From this measurement and equations 5, 6, or 7 the noise temperature can then be computed.

Crystal Transient Reduction

During a given liquid helium run the crystal will be excited many times above the noise level to obtain a measurement of its frequency and Q. An accurate frequency and Q measurement is needed for noise measurements. However, this transient can interfere with the noise measurements. Waiting for it to die away could take a long time if the Q is high. The amplitude decay time, τ_o, is 8 1/6 hours for the silicon described in Table I. For the sapphire $\tau_o = 990$ seconds. Thus to decay by a factor of 10^6 the silicon requires 4.7 days, while the sapphire needs only 3.8 hours. Therefore, measurements of the silicon noise will be delayed for a substantial amount of time. With the present Q noise measurements of the sapphire will not be substantially delayed by its excitation transient. However, future transducers, capacitive or inductive instead of ceramic piezoelectric, will by design produce much higher Q's for all crystals. This section briefly discusses some ways to reduce the transient itself or its effects on the noise measurement.

The crystal is excited by applying a sinusoid voltage at the crystal frequency across C_2 (figure 3) for a short interval of time. The transient can then be reduced by applying another sinusoid of appropriate phase and duration. This technique has been tried successfully with the silicon bar at liquid helium temperatures. However, it does not enable one to closely approach the noise energy of the crystal due to the relatively large amounts of wideband noise compared to the low level of noise energy expected in the crystal. Reducing the bandwidth does decrease the wideband noise, but also increases the response time of the filters. This means waiting a long time to get information about the phase and amplitude of the transient. For the silicon described by Table I as the transient approaches the level of the noise

energy in the crystal, the time constants of the filters needed to resolve it exceed the damping time of the antenna. Thus this method will not eliminate the lowest levels of the transient.

A second method for reducing the transient is to increase the damping by adding an external resistor across C_2. However, unless C_2 can be made effectively smaller (increased coupling), significant energy from the crystal cannot be dissipated by the resistor. This can be done by adding an appropriate inductor across C_2 also. In order to reduce the transient to the level of the energy noise, the resistor and probably also the inductor will have to be cooled to the same temperature as the crystal. Katsunobu Oide and others at the University of Tokyo have used feedback to reduce the noise temperature of a resistor.[1] This technique might be applicable to removing the transient from high Q, low coupling crystals, but the detailed analysis has yet to be done by this author. After the transient is gone the external resistor and inductor must be removed to make the noise measurement.

Electronic filtering, either digital or analog can reduce the interference caused by the transient energy in the crystal when noise measurements are made. The x and y outputs of the excited crystal have the following form:

$$x(t) = x_n(t) + x_e\, e^{-t/\tau_o}$$

$$y(t) = y_n(t) + y_e\, e^{-t/\tau_o}$$

The subscript "n" refers to the noise discussed in the previous section, and the subscript "e" refers to the excitation of the crystal above equilibrium at some initial time. The ensemble average outputs are then given by,

$$\langle x^2(t) + y^2(t) \rangle = \langle x_n^2 + y_n^2 \rangle + (x_e^2 + y_e^2)\, e^{-2t/\tau_o}$$

$$\langle \dot{x}^2(t) + \dot{y}^2(t) \rangle \tau_f^2 = \langle \dot{x}_n^2 + \dot{y}_n^2 \rangle + \left(x_e^2 + y_e^2\right) \frac{\tau_f^2}{\tau_o^2} e^{-2t/\tau_o}$$

$$\langle (x(t) + \dot{x}(t)\tau_o) + (y(t) + \dot{y}(t)\tau_o)^2 \rangle =$$

$$\langle (x_n + \dot{x}_n \tau_o)^2 + (y_n + \dot{y}_n \tau_o)^2 \rangle$$

Note that the third linear filter totally removes the excitation transient of the crystal before squaring. In practice the crystal decay time, τ_c, will not be known well enough to remove all the transient. Suppose τ_c' is the value which is used for τ_c. Then the following term must be added to the latter equation above,

$$\left(x_e^2 + y_e^2\right)\left(1 - \frac{\tau_c'}{\tau_o}\right)^2 e^{-2t/\tau_o}$$

For the present silicon and transducer one or more of the above methods can be used to remove the transient if an attempt at measuring the energy noise is made. Increased coupling will improve the effectiveness of these techniques.

Reference Frequency

The lock in amplifier requires a reference oscillator. The results of the noise calculations — equations 5, 6, and 7 — are valid only for the reference frequency sufficiently close to the crystal resonance. When the filter time constant is roughly equal to the decay time of the crystal, it turns out that for all three of the linear filters considered the following condition must be maintained, $\left| \frac{\omega_c - \omega_r}{\omega_c} \right| \ll \frac{1}{Q}$

The crystal frequency must be measured to better than this accuracy. The reference must be tuned to and maintained at this frequency to better than this accuracy throughout the duration of the measurement. Data must be collected for a time greater than the decay time of the crystal. Thus the stability and accuracy requirements for each of the crystals is,

silicon, accuracy and stability of better than one part in 3×10^8 over a time greater than 8 hours.

sapphire, accuracy and stability of better than one part in 6×10^7 over a time greater than $\frac{1}{4}$ hour.

Devices are commercially available which have the needed stability and accuracy. They cost several thousands of dollars to buy and several hundred of dollars per month to rent. These alternatives might be considered.

Frequency measuring and generating devices of sufficient accuracy and stability have been constructed from equipment which we already have in our possession. The Hewlett Packard 10544A 10 Mhz quartz crystal oscillator has a rated stability of better than one part in 2×10^9 per day. The oscillator and the HP 5216A electronic counter have the needed precision to measure the

crystal frequencies. The 10 Mhz oscillator is also used to generate the reference frequency. This eliminates the need for calibration. Figure 5 shows the phase lock loop which has been used. Note that the 10 Mhz oscillator is not in the loop. A second crystal oscillator is servoed by a voltage which is proportional to the difference between the desired and the generated periods. Prototypes of this frequency synthesizer have been successfully tested for both silicon and sapphire frequencies.

The frequency of the crystal is a function of temperature. McGuigan and others have determined that at liquid helium temperatures the temperature dependence of the resonance frequency of silicon has the following form.[2]

$$\frac{f(T) - f(0)}{f(0)} = 1.82 \times 10^{-10} T^3$$

During a typical run with the cryostat to be used to make our noise measurements the temperature of the experiment changed from 4.4 Kelvin to 5.7 Kelvin over the six day holding period of the dewar. The best temperature stability was about .1 Kelvin per day for the first four days. An adequate noise measurement requires collecting data for a time equal to many decay times. Ten decay times for the silicon is 3.4 days. During this time the frequency of the silicon will drift by about one part in 3×10^5. Thus the best temperature stability is just at the edge of what is needed. Improvements have recently been made in the cryostat which are expected to increase the thermal stability, ie. better heat sinking of the wires going to the experiment. However, this has not yet been tested. Active temperature control can be provided if necessary. Alternatively if the temperature dependence of the frequency is known accurately enough, the reference frequency can be compensated to follow the crystal frequency.

The temperature dependence of the resonance frequency of sapphire has not yet been obtained by this author. Such data has probably been obtained by V. Braginsky. We hope to obtain it in the near future from him or our own measurements. However, the frequency stability requirements for the sapphire presently being tested are less stringent than for silicon by a factor of over 100. Thus noise measurements for the sapphire probably won't need improved temperature stability or compensation.

Gain and Bandwidth

Careful choice of gain and bandwidth of the stages of the electronics of figure 4 is needed to obtain an adequate output without saturation. Consider first a specific example, $x^2 + y^2$ for the sapphire. For a .7 volt rms output for each of x and y a total gain of 10^{10} is needed. The gain in the low pass filters should be no more than 100 due to dc drifts. Thus the gain of the preceeding stages should be greater than 10^8. The detectors of the lock in amplifier (a PAR 129) begin to saturate at about one volt rms of noise. The narrowband signal will not cause these detectors to saturate but the wideband noise might. The effective noise bandwidth of the preamp and postamp which will not produce this saturation is given by

$$10^8 \times 2 \frac{nv}{\sqrt{hz}} \times \sqrt{\Delta f} < 1 \text{ volt}$$

assuming 2 $nv/\sqrt{hz}$ wideband noise at the preamp input. Thus we need $\Delta f < 25$ hertz. This narrow bandwidth at 18642 hertz might just barely be attainable by the four cascaded LC tuned amplifiers of the postamp. This device presently has a bandwidth of about 78 hertz. More careful tuning and slight amounts of positive feedback might bring the bandwidth down some more.

Table III gives the expected upper limit for the postamp bandwidth for silicon and sapphire and each of the three linear filters. With the possible exception of sapphire at 25 hz = Δf, amplifiers with quartz crystal filters or a combination of down conversion and crystal filters will probably be needed to achieve these narrow bandwidths.

Conclusion

The noise measurement for the sapphire appears feasible with a moderate effort put into further electronic development. The major work which remains to be done is the development of a postamp with narrow enough bandwidth. It is well within technical feasibility.

The noise measurement for the silicon is more difficult, due mainly to the low coupling. Much more development is needed than for the sapphire. It might be more feasible to improve the coupling instead. This would relax the present requirements for transient removal, frequency and temperature stability, and bandwidth by giving a larger energy noise signal and permitting a smaller filter time constant to be used.

Larger couplings can be achieved with piezoelectric transducers and epoxy, but this reduces the Q. As a consequence the Brownian motion noise of the crystal comes more from loss processes in the transducer than from the crystal (and its suspension). The sapphire presently being used had a Q of 4×10^8 at 4 Kelvin before the piezoelectric was attached. The present Q of 58×10^6 means that at equilibrium roughly 15% of the energy noise to be observed comes from the crystal (and its suspension). Possible future experiments with these crystals could have β's as large as 10^{-7} with inductive and capacitive transducers while maintaining high Q. These would, however, require separations of about .1 mm between the transducer and the end of the crystal. The use of a properly matched SQUID amplifier instead of an FET would also be a significant improvement.

REFERENCES

1) Katsunobu Oide, Yujiro Ogawa, and Hiromasa Hirakawa, "Artificial Cold Resistors," Japanese Journal of Applied Physics, 17,429 (1978).

2) D.F. McGuigan, C.C. Lam, R.Q. Gram, A.W. Hoffman, D.H. Douglass, and H.W. Gutche, "Measurements of the Mechanical Q of Single-Crystal Silicon at Low Temperatures," Journal of Low Temperature Physics, 30, 621 (1978).

TABLE I

PROPERTIES OF MONOCRYSTALS COUPLED TO TRANSDUCERS

material	mass (kg)	length (cm)	fundamental mode frequency at 5 Kelvin (hz)	loaded Q at 5 Kelvin	β at 5 Kelvin
Silicon	15½	135	3467.8	320×10^6	$\lesssim 10^{-9}$
Sapphire	5.2	25	18,642	58×10^6	$\gtrsim 10^{-7}$

	τ_0 (sec)	L_1 (henries)	$R_1 + R_2$ (ohms)	C_1 (farads)	C_2 (farads)	$\frac{\beta kT}{C_2}$ (volts)^2
Silicon	29,400	$\lesssim 3 \times 10^9$	$> 2 \times 10^5$	$\lesssim 7 \times 10^{-19}$	7.0×10^{-10}	$\lesssim (10^{-11})^2$
Sapphire	990	8.1×10^3	1600	9.0×10^{-17}	9.0×10^{-10}	$(88 \times 10^{-12})^2$

TABLE II

Expected Values of τ_f and Noise when Wideband Noise Equals Narrowband Noise

		$x^2 + y^2$	$(\dot{x}^2 + \dot{y}^2)\ \tau_f^2$	$(x + \dot{x}\tau_o)^2 + (y + \dot{y}_o)$
Silicon	τ_f (sec)	28,000	111,000	44,300
	total noise referred to preamp input (volts)	10^{-11}	5×10^{-12}	8×10^{-12}
Sapphire	τ_f (sec)	216	890	590
	total noise referred to preamp input (volts)	10^{-10}	6×10^{-11}	7×10^{-11}

TABLE III

Expected Upper Limit of Postamp Bandwidth to Prevent Saturation of Lock-in Amplifier

	$x^2 + y^2$	$(\dot{x}^2 + \dot{y}^2)\ \tau_f^2$	$(x + \dot{x}\tau_o)^2 + (y + \dot{y}\tau_o)^2$
Silicon Δf (hertz)	.25	.063	.16
Sapphire Δf (hertz)	25	9	12

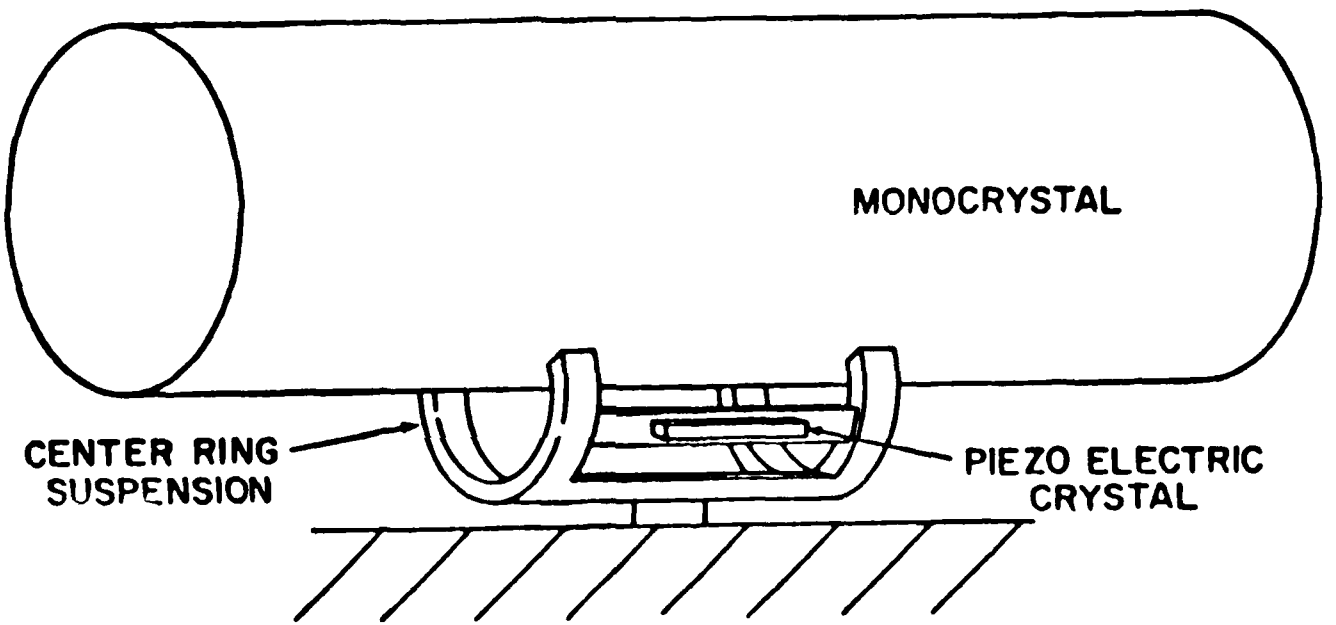

Figure 1

Silicon Suspension

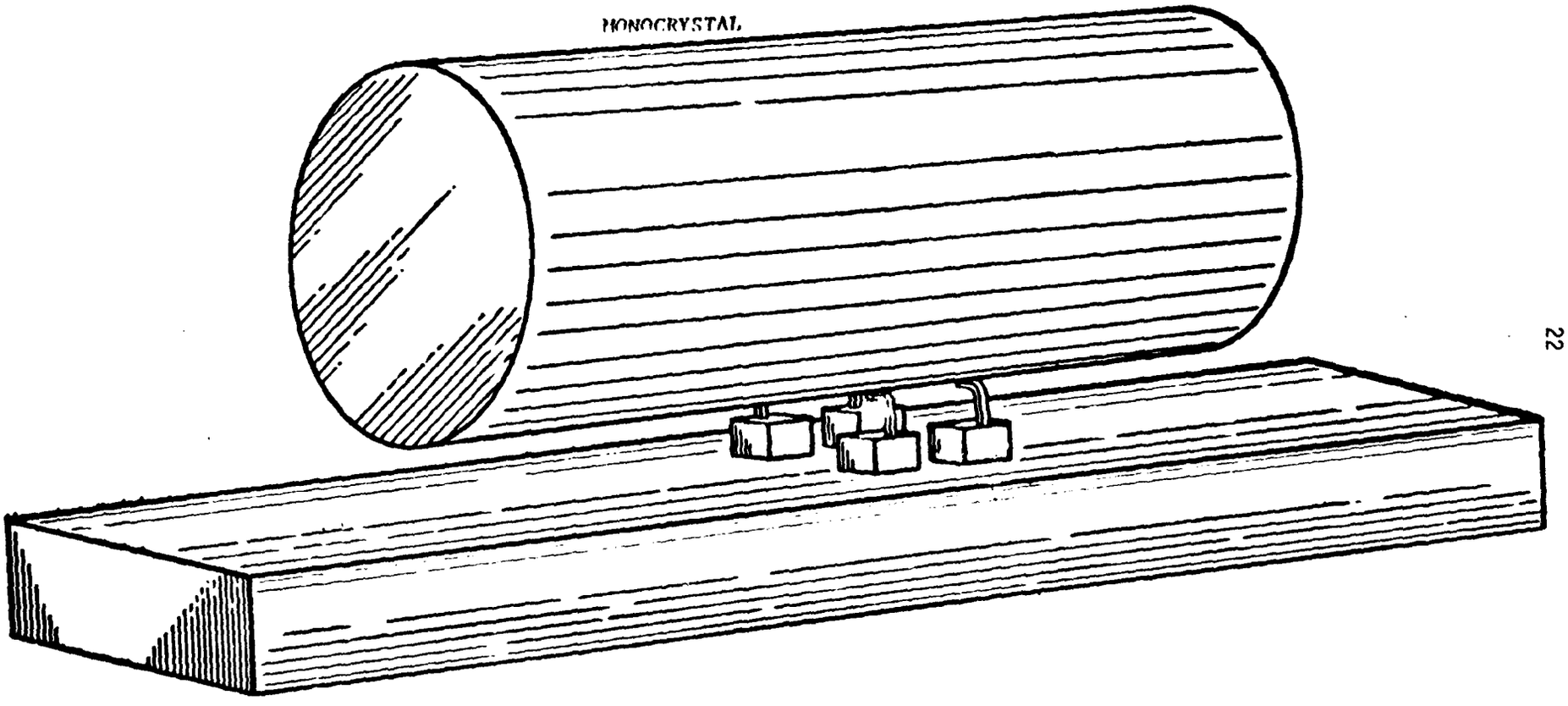

Figure 2

Sapphire Suspension

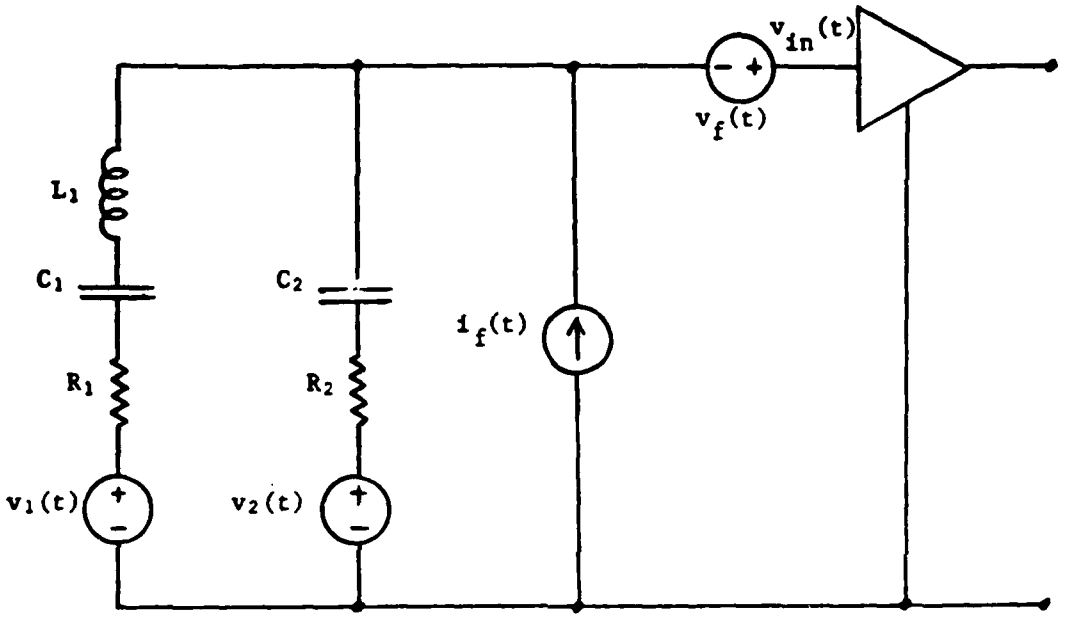

$\omega_0^2 = \frac{1}{L_1}\left(\frac{1}{C_1} + \frac{1}{C_2}\right)$ resonant frequency

$\beta = \frac{C_1}{C_1 + C_2}$ coupling

$\tau_0 = \frac{2L_1}{R_1 + R_2}$ amplitude decay time

$Q = \frac{\omega_0 L_1}{R_1 + R_2}$ quality factor

$1 = L_1 C_2 \omega_0^2 \xi$

	Time Domain	Spectral Density
crystal noise	$v_1(t)$	$e_1(\omega)$
transducer noise	$v_2(t)$	$e_2(\omega)$
amplifier noise	$v_f(t)$	$e_f(\omega)$
	$i_f(t)$	$j_f(\omega)$

$$\langle v^2 \rangle = \int_0^\infty e^2(\omega)\, d\omega \qquad \langle i^2 \rangle = \int_0^\infty j^2(\omega)\, d\omega$$

Figure 3, Equivalent Circuit and Definitions

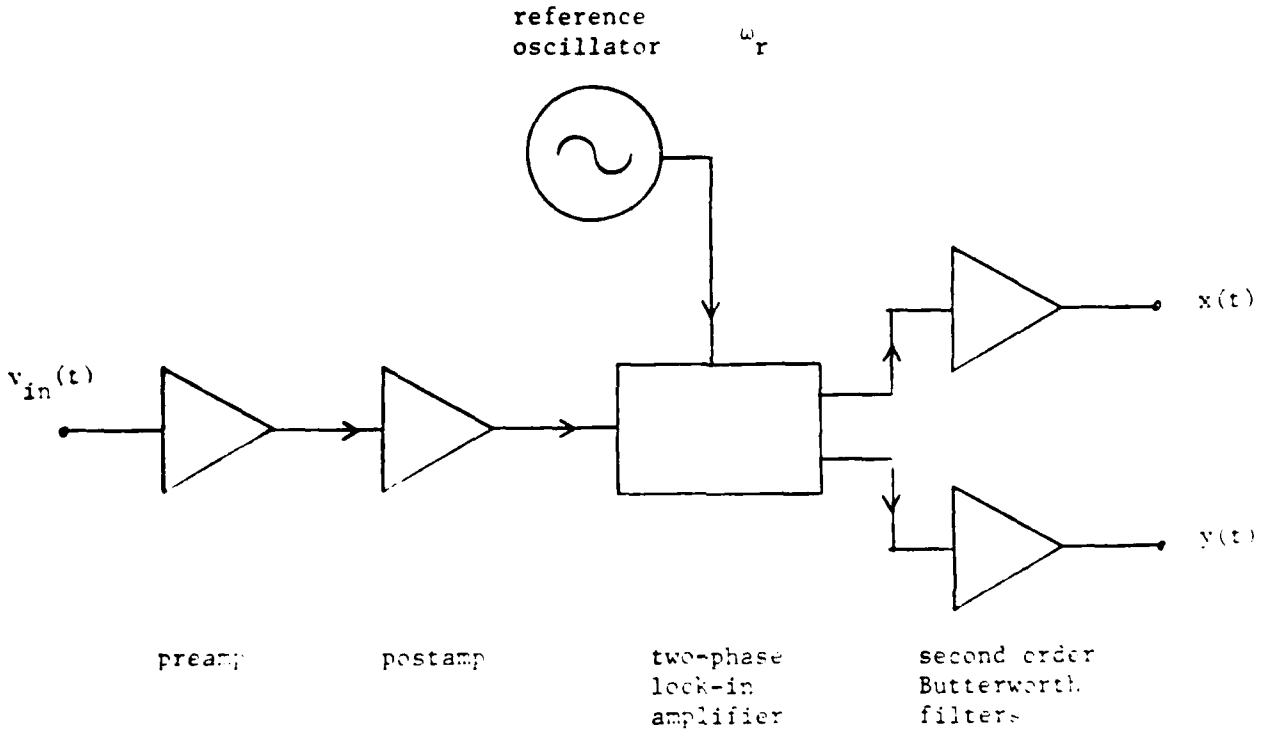

Figure 4, Electronics

x and y may be recorded directly on magnetic tape or undergo further analog processing before being recorded.

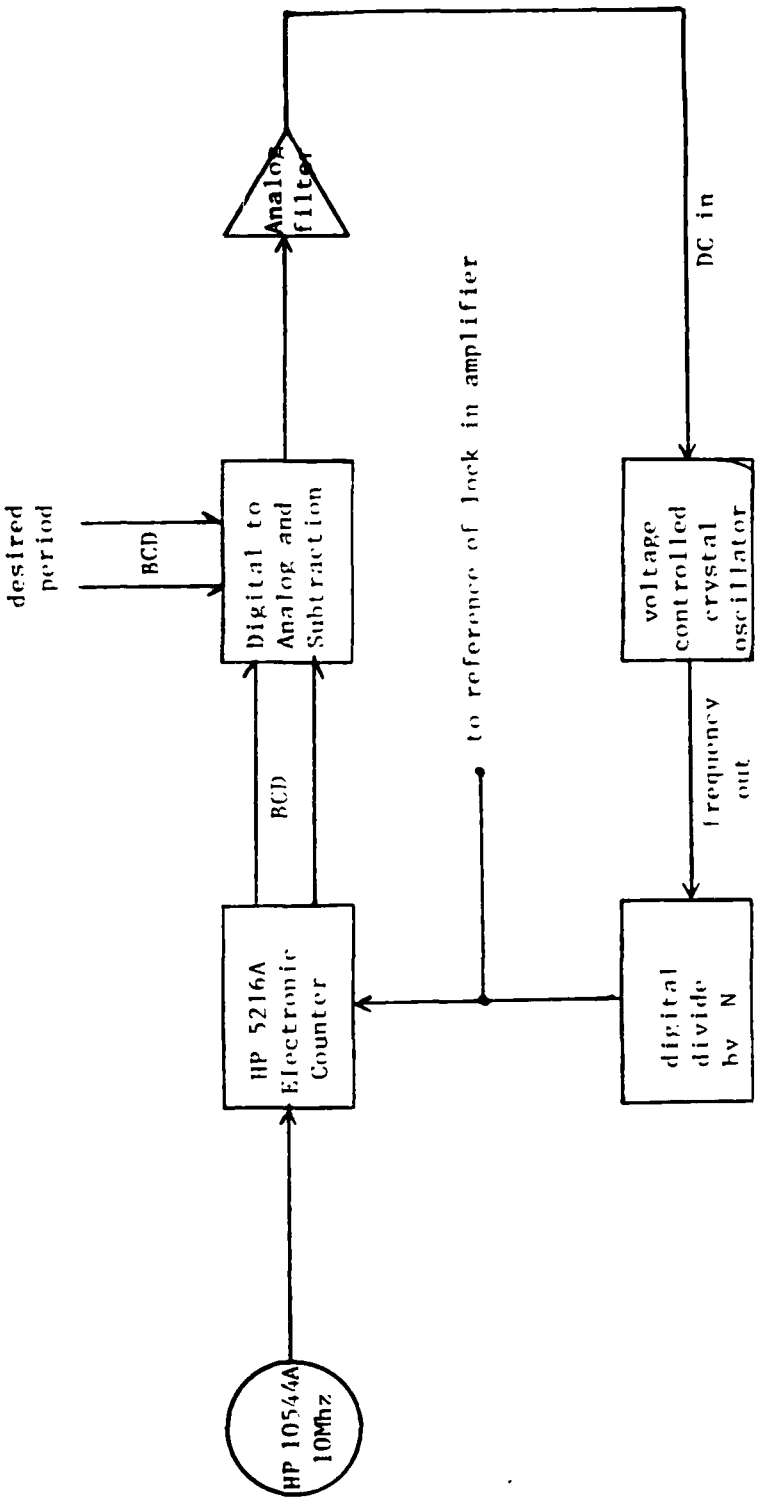

Figure 5. Phase lock loop for generating reference for noise measurements of crystals